[American Journal of Science, Vol. 316, June, 2016, P. 542–577, DOI 10.2475/06.2016.02]

COSMOGENIC-NUCLIDE EXPOSURE AGES FROM THE PENSACOLA MOUNTAINS ADJACENT TO THE FOUNDATION ICE STREAM, ANTARCTICA

GREG BALCO*,†, CLAIRE TODD**, KATHLEEN HUYBERS***, SETH CAMPBELL§, MICHAEL VERMEULEN**, MATTHEW HEGLAND**, BRENT M. GOEHRING§§, AND TREVOR R. HILLEBRAND***

ABSTRACT. We describe glacial-geological observations and cosmogenic-nuclide exposure ages from the Schmidt, Williams, and Thomas Hills in the Pensacola Mountains of Antarctica adjacent to the Foundation Ice Stream (FIS). Our aim is to learn about changes in the thickness and grounding line position of the Antarctic Ice Sheet in the Weddell Sea embayment between the Last Glacial Maximum (LGM) and the present. Glacial-geological observations from all three regions indicate that currently-ice-free areas were covered by ice during one or more past ice sheet expansions, and that this ice was typically frozen to its bed and thus non-erosive, permitting the accumulation of multiple generations of glacial drift. Cosmogenic-nuclide exposure-age data from glacially transported erratics are consistent with this interpretation in that we observe both (i) samples with Holocene exposure ages that display a systematic age-elevation relationship recording LGM-to-present deglaciation, and (ii) samples with older and highly scattered apparent exposure ages that were deposited in previous glacial-interglacial cycles and have experienced multiple periods of surface exposure and ice cover. Holocene exposure ages at the Thomas and Williams Hills, upstream of the present grounding line of the FIS, show that the FIS was at least 500 m thicker prior to 11 ka, and that 500 m of thinning took place between 11 and 4 ka. However, exposure-age data from the Schmidt Hills, downstream of the present grounding line of the FIS, show no evidence for LGM thickening of the FIS and, in fact, provide some evidence that the FIS could have been no more than 200 m thicker than present at the LGM. If all these observations are correct, they imply that the LGM and early Holocene ice surface slope in the vicinity of the present grounding line was steeper than present, which is inconsistent with glaciological model predictions of possible LGM ice sheet configurations. Specifically, scenarios in which the LGM grounding line of the FIS advanced to the outer continental shelf appear inconsistent with exposure-age data from the Schmidt Hills, whereas scenarios in which the FIS grounding line did not advance at the LGM appear inconsistent with exposure-age data from the Williams and Thomas Hills.

Keywords: Antarctica, Pensacola Mountains, Foundation Ice Stream, Last Glacial Maximum, exposure dating, cosmogenic-nuclide geochemistry, glacial geology

INTRODUCTION

This paper describes glacial-geological observations and cosmogenic-nuclide exposure ages in the Schmidt, Williams, and Thomas Hills, which are located in the Pensacola Mountains of Antarctica adjacent to the Foundation Ice Stream (FIS; fig. 1). The FIS drains ice from both the East and West Antarctic Ice Sheets into the Ronne-Filchner Ice Shelf and thence into the Weddell Sea. These exposure-age data are important because they provide information about past changes in the thickness of the FIS, which, in turn, are related to past changes in the thickness and grounding line

* Berkeley Geochronology Center, 2455 Ridge Road, Berkeley, California 94709, USA
** Geosciences, Pacific Lutheran University, Tacoma, Washington, USA
*** Earth and Space Sciences, University of Washington, Seattle, Washington, USA
§ Climate Change Institute, University of Maine, Orono, Maine, USA
§§ Earth and Environmental Sciences, Tulane University, New Orleans, Louisiana, USA
† Corresponding author: balcs@bgc.org

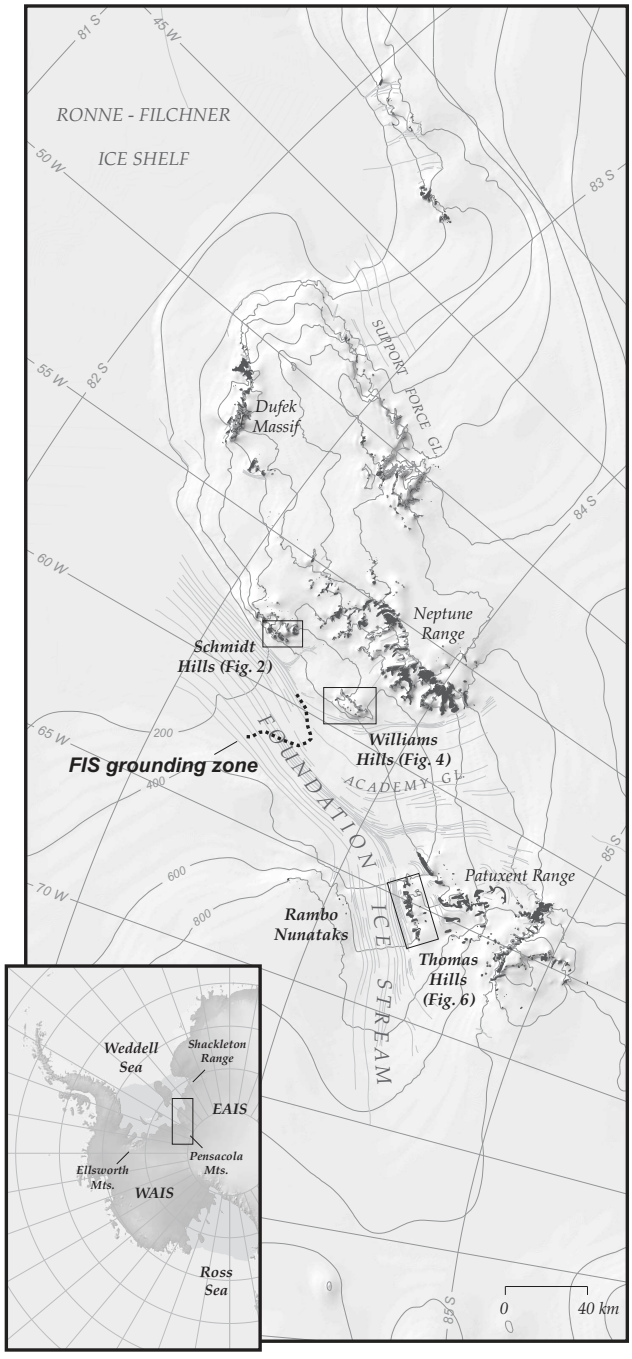

Fig. 1. Map of the Foundation Ice Stream and the Pensacola Mountains. Inset shows location; black boxes show locations of figures 2, 4, and 6. Vector map data are from the Antarctic Digital Database; shaded-relief background image is generated from the RAMP digital elevation model (Liu and others, 2001). The location of the FIS grounding zone is from Rignot and others (2011a, 2011b).

position of the Antarctic Ice Sheet in the Weddell Sea embayment. Specifically, our aim in this project is to learn about changes in the thickness of the FIS between the Last Glacial Maximum (LGM) approximately 15,000 to 25,000 years ago, when the Antarctic ice sheets were significantly larger than now, and the present time.

Hillenbrand and others (2014) reviewed existing geological and geochronological constraints on LGM-to-present changes in ice thickness and grounding line position in the Weddell Sea embayment; in this paragraph we summarize their review. Mainly, these constraints include radiocarbon dates on glaciomarine and marine sediment from the continental shelf north of the present ice shelf edge as well as cosmogenic-nuclide exposure ages from the Ellsworth Range west of our study area and the Shackleton Range to the northeast. Hillenbrand and others considered the marine radiocarbon data to be most consistent with a scenario in which the LGM grounding line advanced to the outer continental shelf, north of the present ice shelf edge and more than 600 km north of its present position, at 25,000 years BP, and grounding line retreat to its present position took place between 25,000 to 5,000 years BP. They pointed out that exposure-age data from the Ellsworth Mountains in the central Weddell embayment, which record several hundred meters of LGM-to-present thinning, are potentially consistent with this reconstruction. On the other hand, they considered (i) exposure-age data from the Shackleton Range on the east side of the Weddell embayment, which show no evidence for thicker LGM ice, as well as (ii) ice-core and ice-penetrating radar data from Berkner Island, which indicate only minor LGM thickening, to be inconsistent with this reconstruction. Hillenbrand and others considered these terrestrial data from the eastern Weddell embayment to be most consistent with an alternative scenario in which the grounding line did not advance to the outer shelf during the LGM, and, in fact, remained close to its present position in the eastern Weddell embayment adjacent to the Shackleton and Pensacola ranges. The purpose of this paper is to describe glacial-geological observations and cosmogenic-nuclide exposure-age data from the southernmost Weddell embayment that are potentially useful in determining which of these possible reconstructions is correct.

GLACIAL GEOLOGY OF THE SCHMIDT, WILLIAMS, AND THOMAS HILLS

Schmidt and Williams Hills

The Schmidt Hills is a group of nunataks near the present grounding line of the FIS with summits near 1100 m, approximately 800 m above the adjacent surface of the FIS (figs. 1, 2, and 3). The Williams Hills is a smaller range of similar nunataks that lies 50 km upstream of the Schmidt Hills below the confluence of the FIS and the Academy Glacier (figs. 1 and 4). The ice surface elevation at the confluence is near 350 m and summits in the Williams Hills are 900 to 1000 m elevation. Both ranges lie in an accumulation zone: exposed portions of nunataks are separated from adjoining glaciers by fringing snowfields and small glaciers that slope away from the peaks and display bergschrunds and active crevassing (figs. 2, 3, and 4). Thus, local snow accumulation is sufficient to drive ice flow away from local summits into the FIS and its tributaries, and ice margins are locally up to several hundred meters higher than the center of the FIS (fig. 3).

Bedrock in the Schmidt and Williams Hills is phyllite-grade metasediment of the Precambrian Patuxent Formation intruded by basalt and metabasalt sills (Schmidt and others, 1978). Bedrock foliation is commonly near-vertical and the bedrock surface is weathered, friable, and frost-shattered. In places, steeply foliated bedrock has been pervasively affected by frost heaving and polygonal cracking, resulting in outcrops that have the appearance of incipient patterned ground. Summits generally display outcropping bedrock, but most hillslopes are overlain by colluvium consisting mainly of

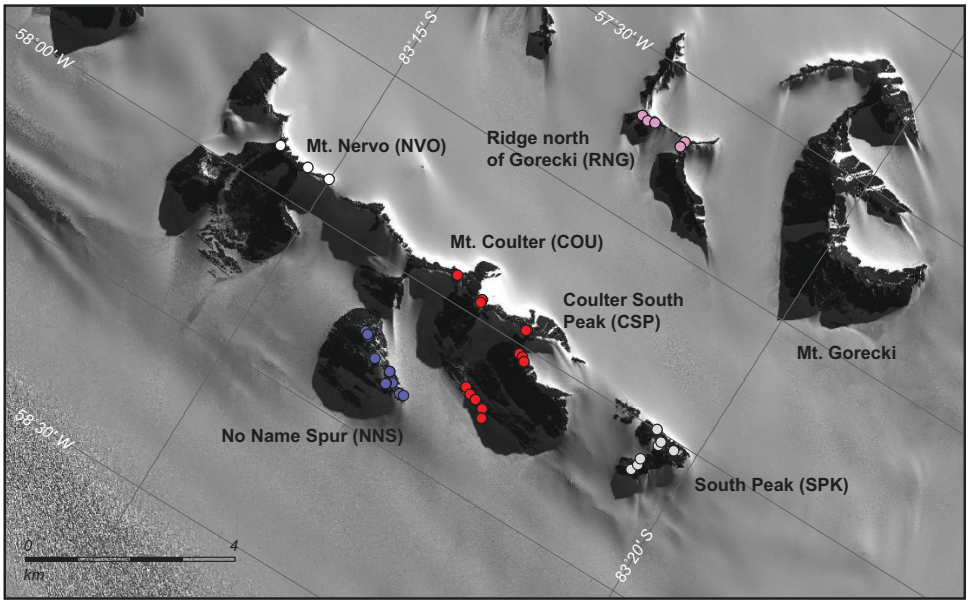

Fig. 2. WorldView-1 satellite image (copyright DigitalGlobe, Inc.) of the southern Schmidt Hills showing sample locations (colored circles). Named sample locations are represented by different colors that match those in figure 10; white circles denote additional samples that were collected but not analyzed. Crevassed area at lower left of image area is the shear zone forming the eastern boundary of the Foundation Ice Stream. No Name Spur and South Peak are informal names.

fragments of locally derived bedrock. In most cases, colluvial aprons on hillslopes display polygonal patterned ground and other evidence of periglacial disturbance (fig. 3).

Bedrock and colluvium are overlain by glacial deposits consisting of sparsely scattered cobbles and boulders, of both exotic lithologies and locally derived bedrock, commonly with evidence of glacial transport such as faceting, polishing, and impact marks (fig. 5). Moraines or any spatially continuous accumulations of drift are absent. Although unconsolidated sediment that forms colluvial aprons on hillslopes locally contains erratic clasts embedded in surface layers, it mainly displays characteristics of colluvium, including predominantly local derivation, evidence of downslope transport, and evidence of periglacial disturbance, and does not display characteristics of glacial till. Erratics are most commonly quartzitic to arkosic sandstones of varying composition and metamorphic grade, presumably mainly derived from the Devonian clastic sequence in the main escarpment of the Pensacola Mountains to the south and east (Schmidt and others, 1978). We found erratics close to the summits of all nunataks we visited. Erratics show a wide range of weathering characteristics ranging from unweathered to heavily oxidized with thick weathering rinds and extensive surface pitting. We found erratics embedded in colluvium, perched on top of colluvium, and perched on bedrock outcrops. In particular, erratics were commonly perched on top of loose surface clasts of felsenmeer derived from fracturing of underlying bedrock.

There is little evidence of glacial erosional features in the Schmidt and Williams Hills. Spurs of nunataks in the Schmidt Hills closest to the FIS (in particular "No Name Spur;" see figs. 2 and 3) are broadly streamlined in shape. We observed three instances in the Schmidt Hills and two in the Williams Hills of weak striations on resistant bedrock knobs (typically upstanding basalt pods), including at one site near the

Fig. 3. View of the southern Schmidt Hills looking south from the summit of Mt. Nervo (see fig. 2). Bedrock exposed at summits is steeply foliated, weathered, and highly friable phyllite-grade metasediment. Hillslopes display colluvium and polygonal patterned ground. Crevassed shear zone in background to right of hills is the eastern margin of the FIS. Spurs closest to the FIS display a coarsely streamlined appearance, but the higher summits do not. The Williams Hills, 50 km to the south, are visible on the horizon to the left of the shear zone. [Photo credit: G. Balco]

summit of Mt Nervo, the highest peak in the Schmidt Hills. In the Schmidt Hills, we observed both range-parallel and range-transverse striations, crosscutting at one site. In the Williams Hills, all striations were range-transverse, that is, perpendicular to the FIS.

These observations, specifically the presence of erratics and striations at all elevations, lead us to conclude that all ice-free areas in the Schmidt and Williams Hills were covered by expanded glacier ice at least once in the past. The presence of erratics with a wide range of weathering characteristics, as well as the presence of erratics perched on top of loose surface debris derived from shattering of friable underlying bedrock, indicates that ice that covered these sites in the past was frozen-based and accomplished minimal subglacial erosion (for example, Sugden and others, 2005). Thus, it is most likely that many of the erratics present have been covered by frozen-based ice one or more times since they were originally emplaced. This situation is commonly observed in Antarctica and presents a particular challenge to exposure-dating studies that aim to find and date evidence of LGM-to-present deglaciation: many past studies have shown that it is generally not feasible based on field criteria to distinguish erratics that were emplaced in the most recent deglaciation from those that have been covered by frozen-based ice one or more times (see discussion in Balco, 2011 and references therein).

Thomas Hills

The Thomas Hills are located an additional 80 km upstream of the Williams Hills, south of the confluence of the FIS and Academy Glacier (figs. 1 and 6). They form an

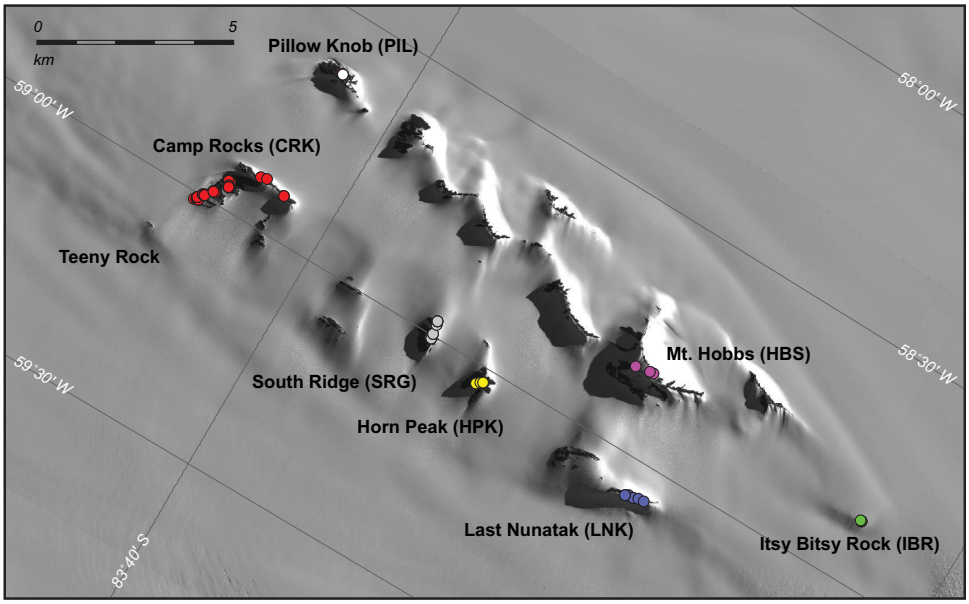

Fig. 4. WorldView-1 satellite image (copyright DigitalGlobe, Inc.) of the Williams Hills showing sample locations (colored circles). Named sample locations are represented by different colors that match those in figure 9; white circles denote additional samples that were collected but not analyzed. The crevassed area in the lower left corner of the image is the eastern boundary of the Foundation Ice Stream. Pillow Knob, Mt. Hobbs, and Teeny Rock are official names; others are informal.

escarpment that separates the higher Macnamara Glacier to the southeast from the FIS to the west. Here the FIS ice surface elevation is near 550 m and Martin Peak, the highest summit in the Thomas Hills, is 1050 m. In contrast to the Schmidt and Williams Hills where local ice margins are well above the level of the FIS, the surface of the FIS slopes toward the Thomas Hills. The ice margin at the western boundary of the Thomas Hills is up to ~75 m below the center of the FIS and is delineated by lobes of blue ice. Thus, the Thomas Hills where they adjoin the FIS are sites of net ablation, and ice is, at present, flowing southeastward away from the FIS toward the ice margin.

Bedrock at the Thomas Hills is similar to that at the Schmidt and Williams Hills, consisting of phyllite-to-schist-grade metapelite with metabasalt sills and pods. The bedrock surface is weathered, friable, and in places affected by frost heaving and polygonal cracking. Some hillslopes in the Thomas Hills are covered by colluvium, primarily composed of locally derived bedrock that displays extensive patterned-ground formation (fig. 7).

Unlike at the Schmidt and Williams Hills, however, significant portions of the Thomas Hills are covered by spatially extensive deposits of glacial sediment. First, on relatively low-angle hillslopes at all elevations throughout the range we observed a fine-grained, matrix-supported till (henceforth, the 'Thomas Hills older till'). The surface of this till is composed of an interlocking cobble pavement with numerous highly weathered boulders of erratic lithologies, mainly quartzitic to arkosic sandstones of varying metamorphic grade, presumably derived from the Devonian clastic sequence in the Pensacola Mountains escarpment to the south and east. We observed oxidation and B-horizon development in this till up to a depth of approximately 40 cm. Boulders on the surface of this till are commonly highly oxidized, spalled, and pitted (figs. 7 and 8).

Fig. 5. Surficial deposits at "Camp Rocks" in the Williams Hills (informal name; see fig. 4). Isolated outcrop in middle distance is Teeny Rock and the shear zone of the FIS is visible beyond in far distance. The prominent light-colored and unweathered erratic at right is sample 10-MPS-099-CRK. Also present are numerous other loose surface clasts, showing a range of surface weathering, oxidation, and pitting, that are primarily fragments of the underlying bedrock but also include erratics of various lithologies. Bedrock is steeply foliated metasediment. [Photo credit: Claire Todd]

Second, at elevations below 560 m in the northern and central Thomas Hills (primarily at Clapperton Ridge, Sugden Ridge, and Mt. Warnke; see fig. 7), we observed accumulations of coarse-grained diamictic drift (henceforth, the 'Thomas Hills younger drift'), primarily composed of erratic lithologies with a fresh, unweathered surface appearance, and variably overlying bedrock, colluvium, and the older till. This drift is only present on the northwest side of the Thomas Hills facing the FIS. Surface clasts on the younger drift are mostly fresh-appearing and lack weathering rinds; polished, faceted, and striated clasts and boulders are common; and the surface of the drift itself is rough at the scale of meters to tens of meters. Although we did not make a comprehensive search for buried glacier ice in this drift, its surface in some places displays extensional cracks and collapse structures characteristic of ice-cored deposits. As part of the Thomas Hills younger drift we group both (i) laterally extensive (hundreds of meters in lateral extent) deposits that form kame-terrace-like accumulations on some hillsides, and (ii) distinct moraines up to several meters thick, several tens of meters wide, and hundreds of meters in length. In places, moraines are draped over one another, indicating emplacement of the stratigraphically younger moraine, presumably by frozen-based ice, without disturbance of the older. A set of cross-cutting moraines that belong to this drift at Sugden Ridge (fig. 6) includes distinct moraines that slope both (i) down from the FIS toward the hills, and (ii) down from the hills toward the FIS, indicating that the Thomas Hills have been both a center of local

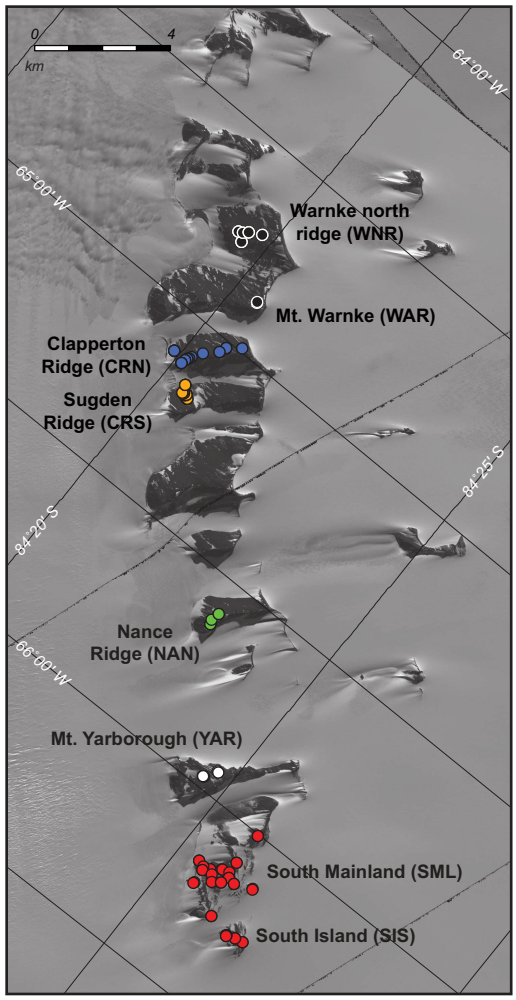

Fig. 6. WorldView-2 satellite image (copyright DigitalGlobe, Inc.) of the Thomas Hills showing sample locations (colored circles). Named sample locations are represented by different colors that match those in figures 14-16. Foundation Ice Stream is to left in image. South Mainland and South Island are informal names.

accumulation and a center of local ablation relative to the FIS at different times in the past.

In addition to the relatively extensive deposits of the older and younger drifts, scattered erratic cobbles and boulders are present throughout the Thomas Hills on bedrock and colluvial surfaces, at all elevations up to several meters below the highest peak in the range, Martin Peak. As is the case for the drifts, lithologies of scattered erratics are mostly sandstones and metasandstones of various composition and metamorphic grade. At lower elevations, we found erratics with a wide range of weathering characteristics, ranging from unweathered clasts with fresh impact marks and other evidence of glacial transport to clasts with thick weathering rinds and pitted surfaces that were often flaked, spalled, and partially disintegrated. In addition, at lower elevations we commonly observed unweathered, striated, and faceted erratic clasts

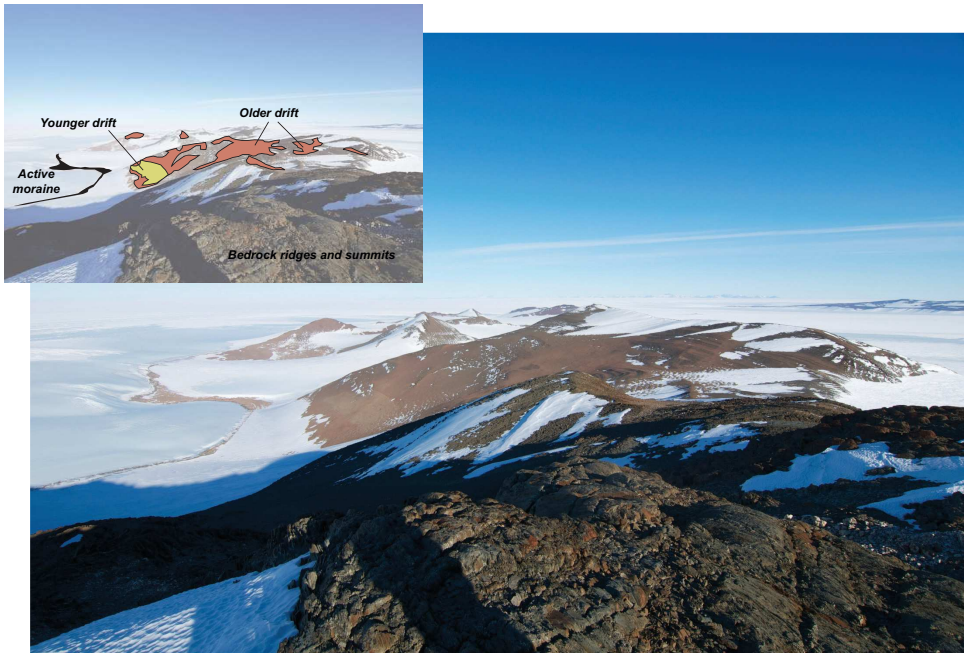

Fig. 7. View of the northern Thomas Hills, looking north from the summit of Mt. Warnke (see fig. 6). The FIS is at left. On hillslopes in center of image, dark-colored areas of outcropping bedrock contrast with smoother, reddish-colored regions that are covered with the Thomas Hills older till. Lighter-colored lobate deposit at left of ridge in middle ground is relatively unweathered and unoxidized Thomas Hills younger drift that overlies the older till. At far left, blue-ice lobes flowing from left to right from the FIS towards the hills are bordered with active ice-cored moraine deposits. The annotated inset image highlights these units. [Photo credit: G. Balco]

perched on top of erratic boulders with heavily weathered, pitted, and oxidized surfaces (fig. 8). At higher elevations and near summits, erratics were sparse and generally weathered in appearance.

Finally, blue-ice lobes flowing away from the FIS and terminating on the west side of the Thomas Hills are bordered by ice-cored moraines that, in most cases, appear to be actively forming at present (fig. 7). These consist of 10 to 20 cm of diamict covering glacier ice and display precariously balanced clasts and collapse structures indicating active disturbance by sublimation of underlying ice.

As at the Schmidt and Williams Hills, evidence of glacial erosion was weak in the Thomas Hills, being limited to small exposures of striated bedrock surfaces at several locations. In most cases, striations were range-parallel, but in rare cases we observed range-parallel striations crosscut by a weakly developed, range-perpendicular set. Some of the striated surfaces we observed displayed weathering rind development that postdated formation of the striations.

These observations lead us to the following conclusions. The presence of erratics at all elevations indicates that all peaks in the range were covered by ice at least once in the past. We interpret the older, fine-grained, matrix-supported till to record overriding of the entire range by thick, wet-based ice at some past time; we hypothesize that the range-parallel set of striations is associated with the emplacement of this till. The younger drift on the west side of the range facing the FIS, as well as fresher-appearing erratics at low elevations, record one or more later fluctuations of the FIS to at least approximately 200 m above the present ice margin elevation. The presence of

Fig. 8. Surface appearance of glacial deposits at the Thomas Hills. Left panel, Thomas Hills older till at Mt. Yarborough (see fig. 6). This is a fine-grained, matrix supported till with subsurface oxidation to a depth of *ca.* 40 cm, as is visible below geologist at top of image. Extensive oxidation of surface clasts gives rise to the red color prominent on hillslopes in the Thomas Hills (see fig. 7). Center panel, surface of Thomas Hills younger drift at 560 m at Clapperton Ridge. This drift is coarse-grained, clast-supported, and the majority of clasts have fresh surfaces lacking oxidation. Right panel, site near present ice margin at South Mainland (see fig. 6) showing a faceted, polished, and unweathered erratic clast of arkosic sandstone perched on a highly oxidized and weathered boulder embedded in underlying till. [Photo credit: G. Balco]

cross-cutting moraines belonging to the younger drift, as well as the clast-supported nature of the younger drift and the fact that it overlies the older drift in places without apparent disturbance of the older drift, indicate that the younger drift was emplaced by frozen-based ice.

METHODS

Cosmogenic-nuclide Measurements

We measured concentrations of cosmic-ray-produced ^{3}He, ^{10}Be, ^{14}C, and ^{21}Ne in quartz extracted from glacially transported erratics. As in many previous such studies (for example, Stone and others, 2003; Sugden and others, 2005; Bentley and others, 2010; Todd and others, 2010; Balco and others, 2013), our goal in measuring cosmogenic-nuclide exposure ages of these samples was to determine the time that they were exposed by ice retreat. Thus, we collected samples whose geomorphic context indicated that they had been englacially transported, emplaced at their present position by melting or sublimation of ice, and not subsequently disturbed. Our criteria for achieving this were as follows. First, clasts that we sampled are 'glacial erratics,' meaning that they showed evidence for glacial transport, including exotic lithology and/or signs of glacial transport such as striae or impact marks. Second, we collected clasts that were perched upon, rather than embedded in, underlying bedrock or surficial materials, indicating that they were unlikely to have been affected by creep or periglacial disturbance after emplacement. Third, we collected clasts in locations to which they could not have been transported by rolling or sliding; in most cases this means they were located on local high points and not at the base of slopes. Nearly all of the samples described in this paper met these criteria. The chief exception is a set of samples collected from ice-cored moraines at the present ice margin for purposes of characterizing the exposure history of clasts in the currently active moraine at the Thomas Hills; the sediment surface at these sites was clearly actively collapsing due to sublimation of underlying ice.

Helium-3.—We measured the concentration of cosmogenic ^{3}He in quartz in the majority of our samples as a means of differentiating samples that were most likely to have been emplaced by ice retreat during the most recent deglaciation (LGM to present) from those that were emplaced in previous glacial-interglacial cycles and repeatedly covered by ice. The premise of this approach is that a ^{3}He measurement, which requires only brief heating under vacuum to extract He from a small (*ca.* 150 mg) aliquot of quartz, is faster and cheaper than the complex wet chemical preparation required for measurements of other cosmic-ray-produced radionuclides such as ^{10}Be or ^{26}Al. On the other hand, helium is gradually lost from quartz samples by thermally activated diffusion, even at Antarctic surface temperatures, so the apparent ^{3}He-in-quartz exposure age of a sample will always underestimate the true exposure age by an amount that depends on the specific diffusion kinetics of the sample and the temperature history that it experienced (Brook and Kurz, 1993; Tremblay and others, 2014a, 2014b). Thus, ^{3}He-in-quartz exposure dating is fast and cheap, but generally inaccurate. Ackert and others (2007) pointed out that these properties were potentially useful in Antarctic exposure-dating applications where, as is the case in this study, a significant fraction of glacially transported erratics at a particular site are likely to predate the most recent deglaciation and have experienced multiple periods of alternating exposure and cover by frozen-based ice. They noted that even if the ^{3}He-quartz system provides inaccurate exposure ages compared to other nuclide-mineral pairs, ^{3}He measurements should be able to easily distinguish between (i) samples that record the most recent deglaciation, so have exposure ages less than 15 to 20 ka, and (ii) samples that have experienced multiple glacial-interglacial cycles and have apparent exposure ages of tens of thousands to hundreds of thousands of years.

This, in turn, would enable them to focus relatively time-consuming and expensive ^{10}Be measurements on the subset of samples most likely to yield unambiguous exposure ages for the most recent deglaciation. Thus, they devised a strategy for identifying and excluding samples that predate the most recent deglaciation by (i) using a large number of ^{3}He measurements in quartz to quickly screen all samples, followed by (ii) slower and costlier ^{10}Be measurements on only the population of samples with the youngest ^{3}He exposure ages. We attempted to apply this strategy in the present study.

We began by crushing samples and sieving the crushed rock to a grain size approximately equivalent to the original size of quartz grains in the samples. For the majority of our samples, which are weakly metamorphosed medium-grained sandstones, we used 0.25 to 0.5 mm or 0.5 to 0.85 mm grain size fractions. We etched these samples in 10 percent HCl at room temperature to remove Fe-oxide coatings, and then selected quartz grains for analysis by inspection under a binocular microscope. As nearly all the samples were quartzitic sandstones, in most cases this involved manually removing a small number of contaminant grains from a sample that predominantly consisted of quartz.

We encapsulated *ca.* 150-mg aliquots of quartz in Ta packets and extracted He by heating under vacuum using a 810-nm laser diode coupled to a coaxial optical pyrometer in a feedback loop controlled by a Watlow PID controller, thus enabling automated control of laser power to maintain a defined extraction temperature. We then purified helium in an automatically controlled ultra-high-vacuum extraction system by reacting released gases with a SAES GP-50 getter at room temperature, freezing remaining noble gases onto a cryogenic trap at 11 K, and then releasing He into the mass spectrometer at 33 K. The mass spectrometer is a MAP-215 sector field instrument (the BGC "MAP-II" system) updated with a continuous dynode electron multiplier and modern counting electronics. We quantified He amounts by peak height comparison with a manometrically-calibrated helium gas standard with ^{4}He/^{3}He = 1630 that we analyzed several times daily. Several analyses of the CRONUS-P pyroxene standard on this system yielded $(5.20 \pm 0.14) \times 10^{9}$ atoms/g ^{3}He (Blard and others, 2015).

Our aim in these analyses was to rapidly identify samples with apparent ^{3}He exposure ages older than the LGM. Thus, we designed our analytical approach to achieve this goal as rapidly and efficiently as possible, and were less concerned with comprehensive quantification of ^{3}He and ^{4}He systematics in all samples. Initially, we performed a number of step heating experiments to establish a heating schedule for He extraction from typical quartz samples that would both ensure complete extraction of cosmogenic ^{3}He and minimize the likelihood of undesired collateral heating of adjacent samples in the laser chamber. Collateral heating is a particular concern due to (i) the high diffusivity of He in quartz, and (ii) the fact that samples in our laser heating apparatus are closely spaced so as to accommodate as many samples as possible, thus minimizing the need to open the vacuum system for sample changes. As expected from measured diffusion kinetics of He (Shuster and Farley, 2005), we found that ^{3}He was completely extracted in a single 15-minute heating step at 500 °C. Specifically, ^{3}He signals in subsequent heating steps at the same or higher temperatures were indistinguishable from the full system blank measured by heating an empty Ta packet in isolation. We also established that this heating schedule did not cause collateral degassing of adjacent samples by interspersing samples with full system blanks consisting of empty Ta packets that were loaded, heated, and analyzed in the same way as those containing quartz samples. Total system blanks were 40,000 ± 13,000 atoms ^{3}He for samples from the Schmidt and Williams Hills analyzed in summer 2012

and 62,000 ± 16,000 atoms ^{3}He for samples from the Thomas Hills analyzed in summer 2013.

Although the majority of ^{4}He was released in the 500° step in most cases, significant quantities were released in subsequent steps at the same or higher temperatures. This difference in behavior of ^{3}He and ^{4}He is unexpected if all He is hosted in quartz. However, although we removed quartz grains showing macroscopic inclusions or adhering refractory minerals, it is likely that because of the expected low U and Th concentrations in quartz, the majority of radiogenic ^{4}He present in these samples is most likely hosted in small U- and Th-rich inclusions that have lower He diffusivity than quartz. On the other hand, we do not expect a significant difference in the cosmogenic ^{3}He production rate between quartz and refractory heavy minerals likely to be present as inclusions, so we do not expect a significant amount of cosmogenic ^{3}He to be present in refractory inclusions. These considerations lead us to hypothesize that release of cosmogenic ^{3}He in our samples dominantly reflects the diffusion kinetics of quartz, but release of radiogenic ^{4}He will be in part controlled by the diffusion kinetics of refractory inclusions. This hypothesis is consistent with our observations, but could be further tested by additional step-degassing experiments as well as sequential dissolution experiments to determine the location of U and Th.

Regardless, these experiments showed that despite retention of some ^{4}He at higher temperatures, cosmogenic ^{3}He is completely released from our quartz samples in a single 15-minute heating step at 500 °C, and we used this heating schedule for all samples. The disadvantage of this procedure, of course, is that we base our assumption of complete ^{3}He extraction on experiments conducted on only a representative subset of samples; we did not verify complete extraction of ^{3}He in each sample by repeat heating steps. We accepted this compromise because our primary goal was to quickly identify samples with ^{3}He exposure ages older than the LGM; if an initial heating step yielded this amount of ^{3}He, release of additional ^{3}He in subsequent steps would not change our conclusion that the sample must have been emplaced before the LGM. Finally, because, as discussed above, this heating schedule does not generally achieve complete degassing of ^{4}He, we only report ^{3}He concentrations.

We assume that all ^{3}He measured in quartz samples is cosmogenic. As noted by Brook and Kurz (1993), the high diffusivity of He in quartz implies that any non-cosmogenic inventory of ^{3}He inherited from the time of mineral formation is unlikely to remain.

Beryllium-10.—We prepared large aliquots of purified quartz from some samples for ^{10}Be, ^{21}Ne, and ^{14}C analysis by repeated etching in dilute HF. We extracted Be in the University of Washington Cosmogenic Nuclide Lab by an isotope dilution method comprising addition of ^{9}Be carrier, complete dissolution in concentrated HF, and Be purification by column chromatography and selective precipitation (Stone and others, 2004). We then measured Be isotope ratios by AMS at the Center for Accelerator Mass Spectrometry, Lawrence Livermore National Laboratory. ^{10}Be concentrations are normalized to the "07KNSTD" Be isotope ratio standards of Nishiisumi and others (2007). Full carrier and process blanks contained 7800 ± 3700 atoms ^{10}Be for samples from the Schmidt and WIlliams Hills processed in 2012 and 15,800 ± 14400 atoms ^{10}Be for samples from the Thomas Hills processed in 2013. This is 0.01 to 1.5 percent of the total number of atoms present for all samples, save two samples with apparent exposure ages less than 1000 years, for which it is 13 to 15 percent of the total number of atoms present.

Neon-21.—We extracted ^{21}Ne from subsamples of the same purified quartz separate used for ^{10}Be analysis by encapsulating *ca.* 150-mg aliquots in Ta packets and step-heating them under vacuum using the laser heating system described above. The gas purification system, processing procedure, and mass spectrometer are the same as

used for the ^{3}He measurements described above, except that Ne was separated from other noble gases by freezing at 33 K, pumping away He, and then releasing Ne into the mass spectrometer at 70 K. Mass-spectrometric measurement of Ne isotopes on this system is described by Balco and Shuster (2009a) and employs a ^{39}Ar spike to correct for the ^{40}Ar++ interference on mass 20. We quantify Ne amounts by peak height comparison with a manometrically calibrated air standard that is analyzed several times daily. Repeated (n = 8) analyses of the CRONUS-A quartz standard on this system during the period of these measurements yielded (333.0 ± 3.3) × 10^{6} atoms/g cosmogenic ^{21}Ne (Vermeesch and others, 2015). Ne isotope compositions in quartz from the Schmidt and Williams Hills were indistinguishable from the atmospheric-cosmogenic mixing line. Thus, we calculated excess ^{21}Ne concentrations with respect to atmosphere; we discuss nucleogenic ^{21}Ne contributions below.

Carbon-14.—We extracted ^{14}C from subsamples of the same purified quartz separate used for ^{10}Be analysis. Samples were dissolved using $LiBO_2$ flux at 1100 °C in the presence of high-purity O_2, followed by cryogenic purification of CO_2 and graphitization, in extraction line 1 at the Purdue Rare Isotope Measurement Laboratory (PRIME Lab). The total amount of ^{14}C is quantified by manometric measurement of total CO_2 released from the quartz, isotope dilution by ^{14}C-dead CO_2, AMS measurement of the $^{14}C/^{13}C$ isotope ratio at PRIME Lab, and $^{13}C/^{12}C$ ratio measurement at the Purdue Stable Isotope Facility. The extraction procedure is described in Lifton and others (2015) and data reduction in Hippe and Lifton (2014). These samples and corresponding blanks were processed prior to adoption of a procedure for He-backfilling of the furnace tube while open to the atmosphere (Lifton and others, 2015). Total system blanks were (1.77 ± 0.33) × 10^{5} atoms ^{14}C (7–11% of total ^{14}C atoms present in the samples). Repeat analyses (n=6) of the CRONUS-A quartz standard on this system yielded (6.89 ± 0.04) × 10^{5} atoms/g ^{14}C (Lifton and others, 2015).

Exposure Age Calculations

We computed exposure ages from cosmogenic-nuclide concentrations using the MATLAB code and "St" scaling scheme of Balco and others (2008), with the Antarctic atmosphere model of Stone (2000). We estimated ^{10}Be production rates due to spallation using the calibration data set of Balco and others (2009). As minor differences between reference production rates inferred from this data set and other recent calibration data sets (Putnam and others, 2010; Kaplan and others, 2011; Young and others, 2013; Heyman, 2014) are not significant to any of our conclusions, we did not consider this issue further. We took the $^{26}Al/^{10}Be$ production ratio to be 6.75 (Balco and others, 2008) and the $^{21}Ne/^{10}Be$ production ratio to be 4.08 (Balco and Shuster, 2009a, 2009b). We estimated ^{14}C production rates using calibration data generated by the CRONUS-Earth project (Borchers and others, 2015) that imply a reference production rate due to spallation of 12.2 atoms g^{-1} yr^{-1} at sea level and high latitude. To calculate apparent exposure ages from ^{3}He concentrations in quartz, we rescaled the production rate measurements of Vermeesch and others (2009) using the same MATLAB code used to compute the exposure ages (that is, the scaling scheme of Stone, 2000), yielding a reference production rate of 116 atoms g^{-1} yr^{-1}. We calculated production rates due to muons using the method of Heisinger and others (2002a, 2002b), as implemented in Balco and others (2008), with muon interaction cross-sections for ^{10}Be taken from data generated by the CRONUS-Earth project (Borchers and others, 2015), for ^{14}C from the data of Heisinger, and for ^{21}Ne from Fernandez-Mosquera and others (2008). We assumed zero production of ^{3}He by muons. Uncertainties in production rates due to muons are not significant to any of our conclusions.

RESULTS AND DISCUSSION

We made a total of 327 cosmogenic-nuclide measurements on 182 samples collected from the Schmidt, Williams, and Thomas Hills. Tables S1 and S2 in the supplementary material (http://earth.geology.yale.edu/%7eajs/SupplementaryData/2016/Balco) show site and sample information, nuclide concentrations, and apparent exposure ages. An "apparent exposure age" is the exposure age calculated for a measured cosmogenic-nuclide concentration under the assumptions that (i) the sample has experienced a single period of exposure at its present location, and (ii) no surface erosion or shielding by snow or sediment has occurred. Complete step-degassing results for cosmogenic ^{21}Ne measurements also appear in the supplementary material (http://earth.geology.yale.edu/%7eajs/SupplementaryData/2016/Balco). Note that some data from the Williams Hills also appear in Tremblay and others (2014a). In addition, complete field and analytical data, photographs, and ancillary material for all samples described in this paper are lodged in the publicly accessible ICE-D: ANTARCTICA database (http://antarctica.ice-d.org).

Williams Hills

Figure 9 shows exposure-age data for the Williams Hills. We began by measuring apparent ^{3}He-in-quartz exposure ages for 37 samples. The majority of these apparent exposure ages are in the range 2 to 5 ka, which is approximately consistent with theoretical expectations for samples that have been exposed during the Holocene given existing estimates of He diffusion kinetics in quartz (Tremblay and others, 2014a) and estimated mean annual temperature (*ca.* –30 °C; Graf and others, 1999). A few samples had significantly higher ^{3}He concentrations (apparent exposure ages of 10–40 ka). These samples presumably have true exposure ages significantly older than the LGM, implying that they experienced multiple periods of exposure and have either been recycled from other locations or, more likely, exposed at their present locations during multiple glacial-interglacial cycles.

We then selected a subset (n = 12) of these samples with relatively young apparent ^{3}He exposure ages for ^{10}Be measurements (fig. 9). ^{10}Be exposure ages range from 4 to 11 ka. At two nunataks where we analyzed multiple samples (Camp Rocks and Last Nunatak; see fig. 9), ^{10}Be exposure ages increase monotonically with elevation. An offset in elevation between samples with the same ^{10}Be exposure age at the two sites is consistent with the present ice surface slope adjacent to the Williams Hills massif: at present, the ice margin at Last Nunatak is 50 m above the ice margin at Camp Rocks, and samples from the two sites that have similar exposure ages of 6 to 9 ka are also offset by 50 m. Likewise, an elevation offset between the youngest exposure ages we observe near the present ice margins at Camp Rocks and Itsy Bitsy Rock is consistent with the present ice surface slope between these locations.

Overall, the ^{10}Be results from the Williams Hills form an internally consistent age-elevation array, from which we conclude the following. First, the ice surface prior to 11 ka was above the local high point at Mt. Hobbs, but we cannot determine the maximum LGM ice thickness in the Williams Hills or the time at which it was reached. Second, steady thinning of the FIS-Academy Glacier region adjacent to the Williams Hills took place between 11 to 5 ka at an average rate near 9 cm yr^{-1} . Data from one site (Camp Rocks; see fig. 9) imply faster thinning at 6.5 to 7 ka than before or after that time, but we have not replicated that with data from other locations.

Schmidt Hills

As at the Williams Hills, we began analysis of Schmidt Hills samples by measuring ^{3}He in quartz in a large number (n = 31) of samples (fig. 10). In general, apparent ^{3}He exposure ages from Schmidt Hills samples are much older than for Williams Hills samples. A few data from the Schmidt Hills fall in the 1 to 5 ka range characteristic of

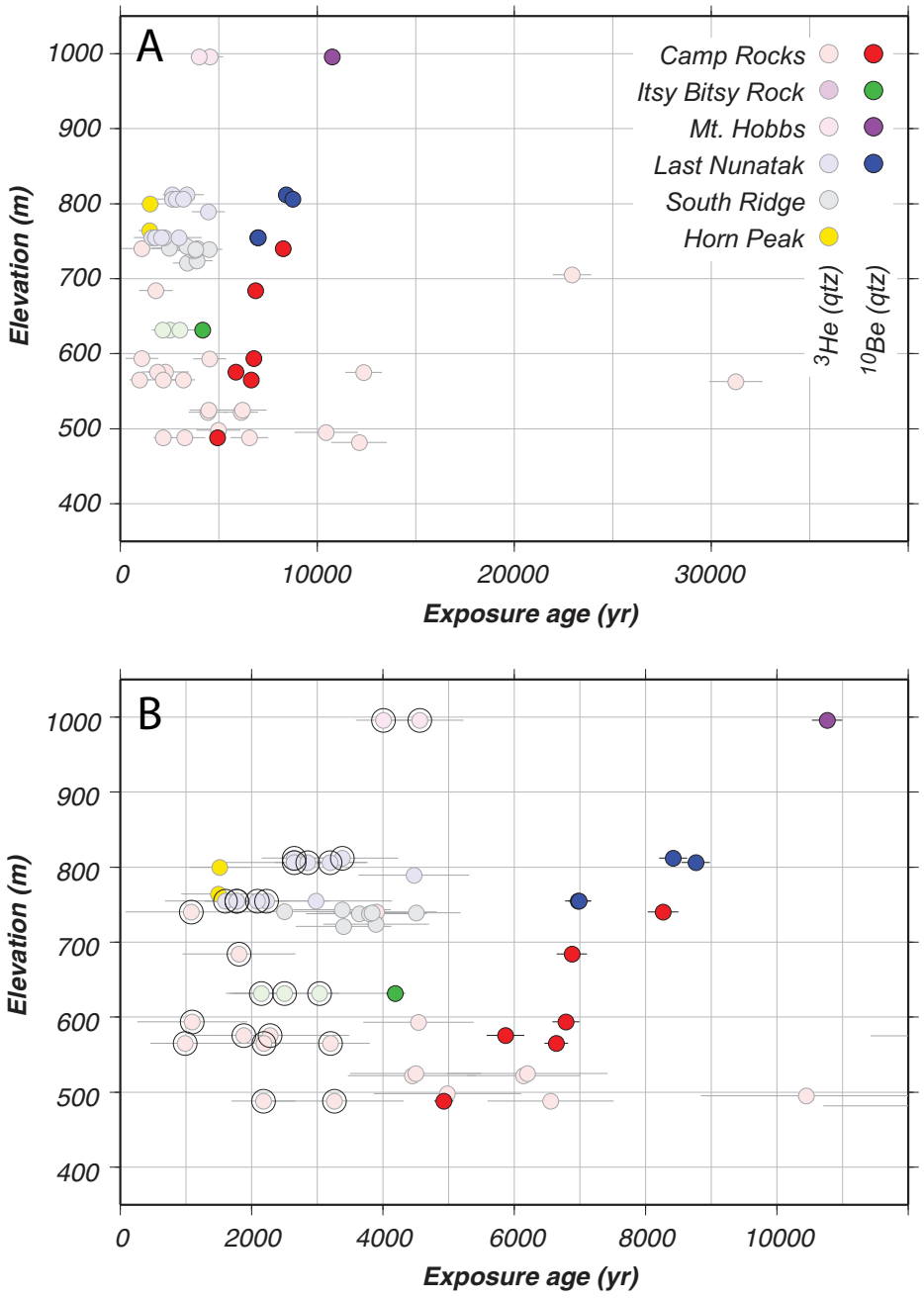

Fig. 9. Apparent ^{3}He-in-quartz and ^{10}Be-in-quartz exposure ages for the Williams Hills. (A) and (B) panels show the same data on different x-axes; A panel includes all data. Colors correspond to named sample sites shown on figure 4. Some samples have multiple ^{3}He measurements, in which case each is shown as a distinct symbol. Error bars are one standard error. As the purpose of this figure is to compare multiple exposure ages from the same location, only measurement uncertainties are shown. In the B panel, dark circles around ^{3}He data indicate the samples for which we also measured ^{10}Be concentrations.

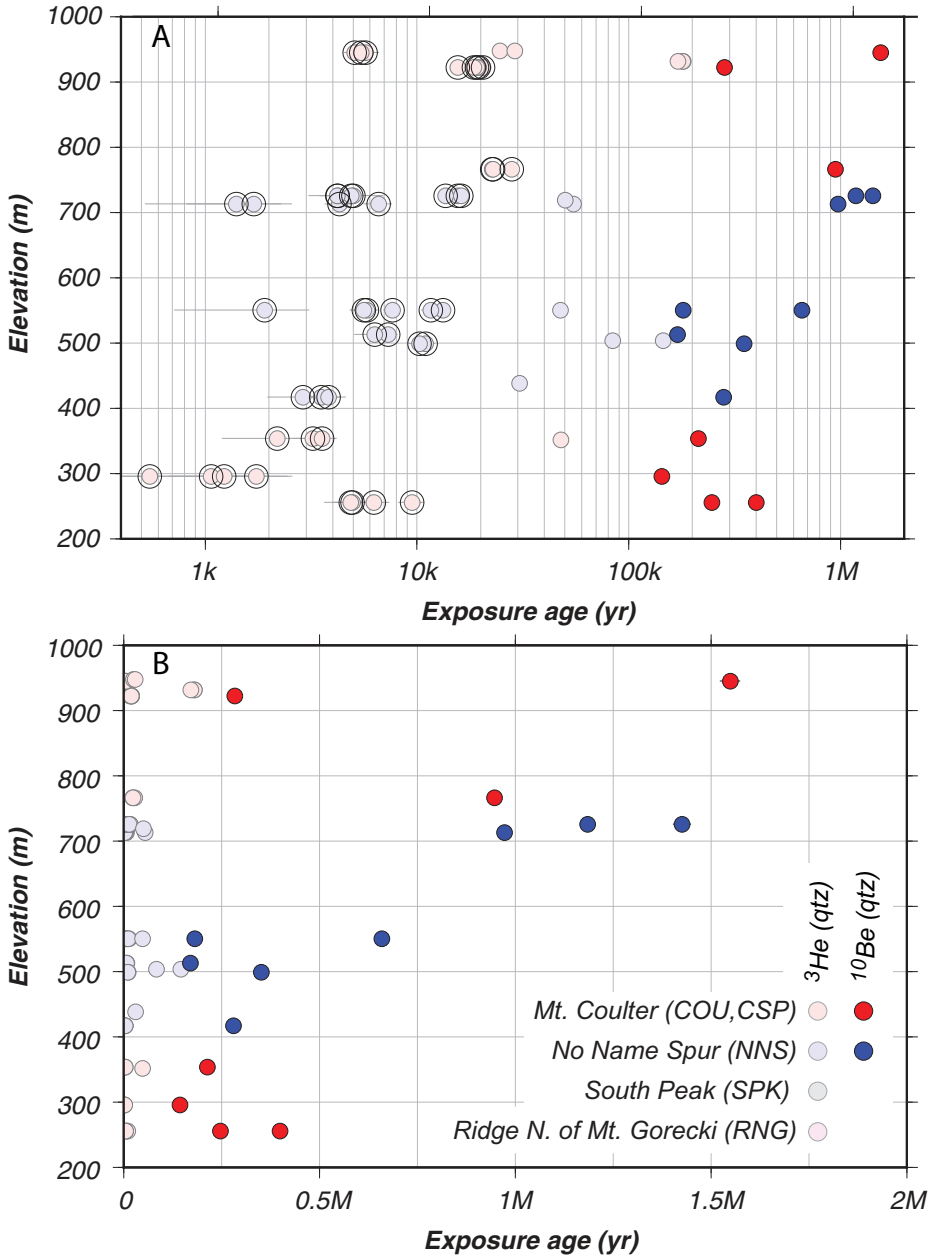

Fig. 10. Apparent ^{3}He-in-quartz and ^{10}Be-in-quartz exposure ages for the Schmidt Hills. Colors correspond to named sample sites shown on figure 2. (A) and (B) panels show the same data on different x-axes. Some samples have multiple ^{3}He measurements, in which case each is shown as a distinct symbol. Error bars are one standard error. As the purpose of this figure is to compare multiple exposure ages from the same location, only measurement uncertainties are shown. In the A panel, dark circles around ^{3}He data indicate the samples for which we also measured ^{10}Be concentrations.

Williams Hills samples, but the majority are older, and we observed apparent ^{3}He exposure ages up to 200 ka. We measured ^{10}Be concentrations in the 15 samples with the youngest apparent ^{3}He exposure ages, which were in the range 1 to 25 ka. Apparent ^{10}Be exposure ages of these samples range from 150 ka to 1.6 Ma (fig. 10). Thus, in contrast to the results from the Williams Hills, neither the ^{3}He or the ^{10}Be exposure-age data provide any evidence that the ice sheet in the vicinity of the Schmidt Hills was thicker than present during the LGM or Holocene.

We also measured cosmogenic ^{21}Ne concentrations in some samples for which we had already measured ^{10}Be concentrations. This is relevant because the ^{10}Be/^{21}Ne production ratio in quartz is fixed by the mineral chemical composition, but ^{21}Ne is stable whereas ^{10}Be is radioactive ($t_{1/2}$ = 1.4 Ma). This relationship makes it theoretically possible to distinguish between a sample that has experienced continuous exposure at the surface (in which case the measured ^{10}Be/^{21}Ne ratio is in equilibrium with the production ratio) and a sample that has been covered by ice for a significant fraction of its exposure history (in which case the measured ^{10}Be/^{21}Ne ratio is significantly less than expected from the production ratio). This basic relationship has been described by many authors (for example, Lal, 1991), and its application to Antarctic bedrock surfaces has recently been reviewed by Balco and others (2014). The ^{10}Be/^{21}Ne ratio is not a particularly sensitive indicator of ice cover. For example, given typical measurement precision for these two nuclides it would be possible to confidently identify a non-equilibrium ^{10}Be/^{21}Ne ratio only if it is approximately 5 percent below equilibrium. Given the 1.4 Ma half-life of ^{10}Be, it would require 102,000 years of ice cover for the ^{10}Be/^{21}Ne ratio to be 5 percent below equilibrium, so it is not possible to unambiguously identify periods of ice cover shorter than this solely from the ^{10}Be/^{21}Ne ratio. Thus, this measurement can be used to show that samples have been covered by ice, because a measured ^{10}Be/^{21}Ne ratio significantly below the equilibrium value requires that the sample has been covered for a significant fraction of its exposure history. However, it cannot be used to prove that samples have never been covered by ice, because a sample with a ^{10}Be/^{21}Ne ratio indistinguishable from equilibrium could have been covered by ice for significant periods of time without perturbing the ratio at a measureable level.

The nuclide concentration measurements in table S1 show concentrations of total excess ^{21}Ne relative to the isotopic composition of atmospheric Ne, which potentially includes both cosmogenic ^{21}Ne and nucleogenic ^{21}Ne derived from U and Th decay (for example, Niedermann and others, 1993). To determine the cosmogenic ^{21}Ne concentration in a sample, therefore, an estimate of the nucleogenic ^{21}Ne concentration is required. We estimated nucleogenic ^{21}Ne concentrations for sandstone lithologies characteristic of our samples by measuring total excess ^{21}Ne concentrations in sandstone erratics from the Williams Hills that had Holocene ^{10}Be exposure ages (fig. 11). If we assume, as implied by the ^{10}Be exposure-age data, that these samples have all experienced a single period of Holocene exposure at their present location, total excess ^{21}Ne concentrations in these samples are nearly two orders of magnitude higher than expected if all excess ^{21}Ne is cosmogenic. We conclude that nearly all excess ^{21}Ne present in these samples is nucleogenic. Note that we cannot exclude the possibility that some of this ^{21}Ne inventory that is not attributable to Holocene exposure is not in fact nucleogenic, but instead cosmic-ray-produced ^{21}Ne inherited from some long past period of exposure at a different location. However, this distinction is not important for the present purposes because we are simply interested in determining how much of the observed ^{21}Ne was not produced by recent (for example, postdating emplacement of the samples at their present locations) exposure, regardless of its source. Nucleogenic ^{21}Ne concentrations computed on this basis (table 1) are 6 to 15 Matoms g^{-1} (excluding two outliers; see fig. 11 and table 1). This range is similar to the nucleo-

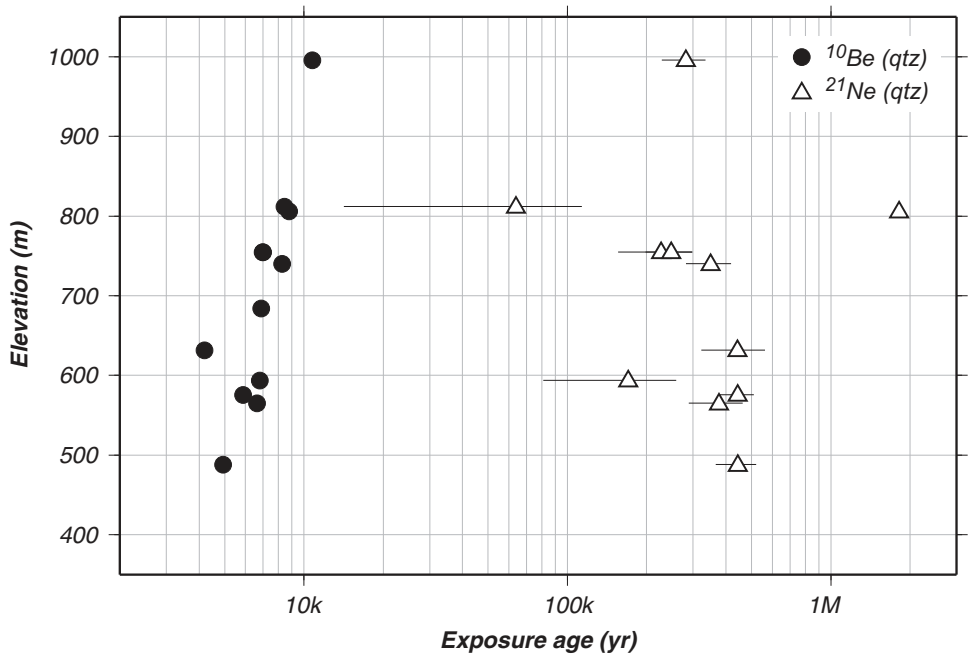

Fig. 11. Apparent exposure ages for sandstone erratics from the Williams Hills based on ^{10}Be (circles) and total excess ^{21}Ne (triangles) concentrations. ^{21}Ne concentrations are much greater than expected from the Holocene exposure history inferred from the ^{10}Be exposure ages, indicating that nearly all of the excess ^{21}Ne inventory is nucleogenic rather than cosmogenic.

genic ^{21}Ne concentration in quartz from Beacon Group sandstones in the McMurdo Dry Valleys of 7.7 ± 2.4 Matoms g^{-1} (Balco and others, 2011; Middleton and others, 2012). All these results are broadly consistent with expected U and Th concentrations in quartz and the Paleozoic age of the sandstones. Thus, we assume in further calculations that quartz in Pensacola Mountains sandstone lithologies contains 12.2 ± 3.4 Matoms g^{-1} nucleogenic ^{21}Ne (table 1).

Table 1

Nucleogenic ^{21}Ne concentrations in Williams Hills sandstone erratics calculated by comparison of ^{10}Be and ^{21}Ne concentrations

Sample name	[^{10}Be] (Matoms g^{-1})	+/-	[^{21}Ne]$_c$ (predicted) (Matoms g^{-1})	+/-	[^{21}Ne]$_{xs}$ (measured) (Matoms g^{-1})	+/-	[^{21}Ne]$_n$ (calculated) (Matoms g^{-1})	+/-
10-MPS-073-CRK	0.0828	0.0023	0.3377	0.0095	14.3	2.8	14.0	2.8
10-MPS-077-CRK	0.0392	0.0012	0.1601	0.0047	14.4	2.5	14.3	2.5
10-MPS-090-CRK	0.0585	0.0018	0.2388	0.0072	6.0	3.1	5.8	3.1
10-MPS-095-CRK	0.0505	0.0025	0.2060	0.0100	15.6	2.3	15.4	2.3
10-MPS-099-CRK	0.0561	0.0015	0.2290	0.0062	13.0	3.0	12.8	3.0
10-MPS-120-IBR	0.0373	0.0012	0.1521	0.0049	16.1	4.4	15.9	4.4
10-MPS-123-HBS	0.1324	0.0028	0.5400	0.0110	14.2	2.7	13.6	2.7
10-MPS-124-LNK	0.0873	0.0022	0.3560	0.0090	2.7	2.1	(2.3)	(2.1)
10-MPS-126-LNK	0.0871	0.0022	0.3554	0.0088	73.8	2.6	(73.4)	(2.6)
10-MPS-128-LNK	0.0692	0.0020	0.2824	0.0081	9.2	2.9	8.9	2.9
10-MPS-129-LNK	0.0677	0.0017	0.2764	0.0068	9.8	2.0	9.5	2.0
Mean and standard deviation (excluding outliers in parentheses)							12.2	3.4

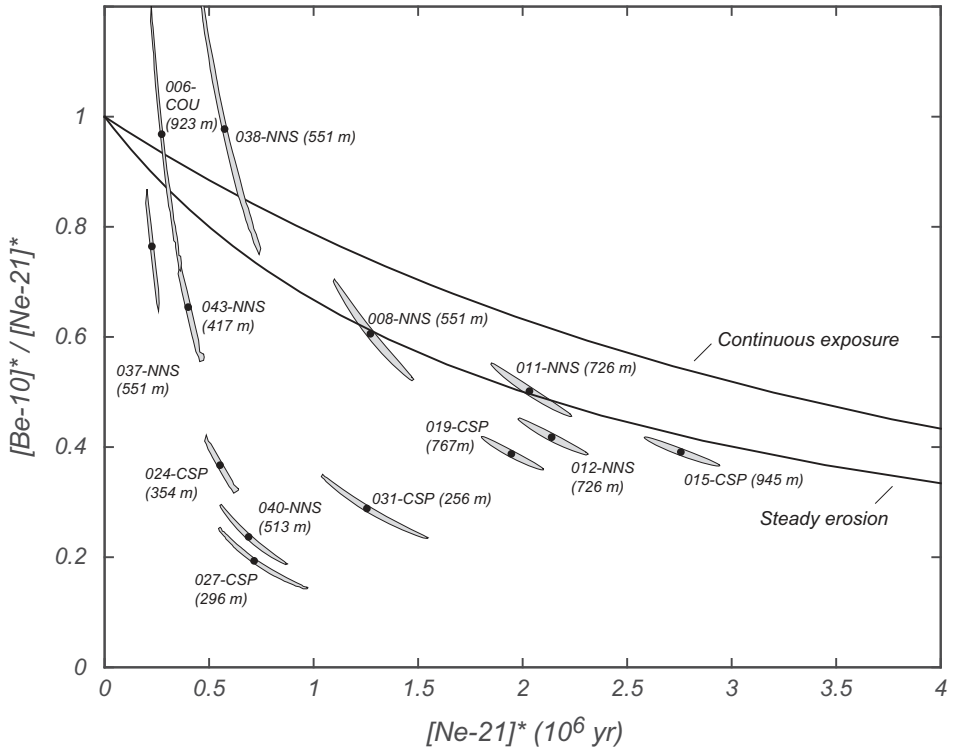

Fig. 12. ^{21}Ne - ^{10}Be/^{21}Ne diagram for sandstone erratics from the Schmidt Hills. The x-axis is the measured ^{21}Ne concentration normalized by the production rate at the site, which has units of years and is equal to the apparent ^{21}Ne exposure age of the sample; the y-axis is the measured ^{10}Be/^{21}Ne ratio normalized to the production ratio (see Balco and others, 2009a, 2009b, 2014 for other examples of this diagram). Black lines are the boundaries of the simple exposure region (Lal, 1991).

Figure 12 and table 2 show cosmogenic ^{21}Ne concentrations and ^{10}Be/^{21}Ne ratios for Schmidt Hills sandstone erratics, that have similar lithology to the Williams Hills erratics, given the assumption that their nucleogenic ^{21}Ne concentration is as calculated above. Some samples with relatively low ^{21}Ne concentrations (at left in fig. 12) have large uncertainties that stem from the nucleogenic ^{21}Ne correction, so provide no useful information. Observed ^{10}Be/^{21}Ne concentrations in the majority of the remaining samples, including at least some samples from the entire range of elevations of the Schmidt Hills, are significantly below equilibrium, indicating that these samples have been covered by ice for a significant fraction of their exposure histories. No discernible relationship between the ^{10}Be/^{21}Ne ratio and sample elevation is present (as we would expect for bedrock samples whose exposure histories must be similar; see Balco and others, 2014), which is consistent with the hypothesis that the samples were emplaced at different times, during different glacial-interglacial cycles spanning a long total length of time. Thus, these observations agree with the conclusion that we draw from the glacial-geological observations, that many if not all erratics in the Schmidt Hills have been repeatedly covered by frozen-based ice during multiple glacial-interglacial cycles, and highlight that the apparent exposure ages of these erratics are very unlikely to represent their true emplacement ages. However, they provide no additional information as to whether or not the Schmidt Hills were ice-covered during the LGM; both possibilities would be consistent with the observations.

TABLE 2

Estimate of cosmogenic ^{21}Ne in sandstone erratics from the Schmidt Hills

Sample name	$[^{21}Ne]_{xs}$ (measured) (Matoms g^{-1})	+/-	$[^{21}Ne]_c$ (calculated) (Matoms g^{-1})	+/-
10-MPS-006-COU	25.4	2.0	13.2	4.0
10-MPS-008-NNS	62.4	3.9	50.2	5.2
10-MPS-011-NNS	93.9	4.0	81.6	5.2
10-MPS-012-NNS	98.0	3.3	85.7	4.7
10-MPS-015-CSP	146.5	4.8	134.2	5.9
10-MPS-019-CSP	92.4	2.3	80.2	4.1
10-MPS-024-CSP	28.0	5.1	15.7	6.1
10-MPS-027-CSP	31.5	3.4	19.3	4.8
10-MPS-031-CSP	43.8	3.4	31.6	4.8
10-MPS-037-NNS	20.1	2.0	7.8	3.9
10-MPS-038-NNS	31.9	2.6	19.7	4.3
10-MPS-040-NNS	35.2	1.9	23.0	3.9
10-MPS-043-NNS	24.4	4.3	12.1	5.5

Because the lack of evidence for LGM ice thickening at the Schmidt Hills is not obviously consistent with the clear evidence for at least 500 m of thickening at the nearby Williams Hills, we investigated this issue further by measuring the cosmogenic ^{14}C concentration in several samples. Unlike the ^{10}Be/^{21}Ne ratio, the ^{14}C concentration in quartz from a bedrock surface sample or, as in this case, an erratic that was presumably emplaced at its present location well before the LGM, provides a means of unambiguously determining whether or not a site was covered by ice at the LGM. Because of the short half-life of ^{14}C (5730 yr), it requires only 30,000 years of continuous surface exposure for the cosmogenic ^{14}C concentration in quartz to become indistinguishable from a "saturated" equilibrium concentration P/λ, where P is the production rate at the site (atoms g^{-1}) and λ is the decay constant of ^{14}C (yr^{-1}). Specifically, it reaches 98 percent of saturation after 30 ka. Thus, a sample that was not covered by ice during the LGM or Holocene will, presumably, have been continuously exposed for more than 30 ka and thus display a saturated ^{14}C concentration. If a sample were ice-covered for a time at the LGM, even if no subglacial erosion took place, ice cover greater than a few meters would halt ^{14}C production and its ^{14}C concentration would be reduced by radioactive decay. If deglaciation occurred 5 to 11 ka as implied by the ^{10}Be exposure ages from the Williams Hills, the subsequent time would not be sufficient to reach saturation again. Thus, an elevation transect of ^{14}C concentrations in quartz would show saturation concentrations at elevations above the LGM ice surface elevation, and concentrations below saturation at lower elevations. Although there is a lower limit on the duration of ice cover that would be detectable using this approach (approximately 1–3 ka, depending on site elevation and measurement precision), the exposure-age data for the Williams Hills indicate that, if the ice thickness history at the Schmidt Hills was similar to that at at the Williams Hills, most parts of the Schmidt Hills would have been ice-covered for at least several thousand years. To summarize, if the LGM-to-Holocene ice cover history at the Schmidt Hills was similar to that at the Williams Hills, this would be evident from ^{14}C concentrations below saturation in Schmidt Hills samples.

Figure 13 shows measured ^{14}C concentrations in three Schmidt Hills erratics and compares them to (i) a theoretical calculation of expected saturation concentrations given the "St" production rate scaling scheme of Balco and others (2008), the Antarctic

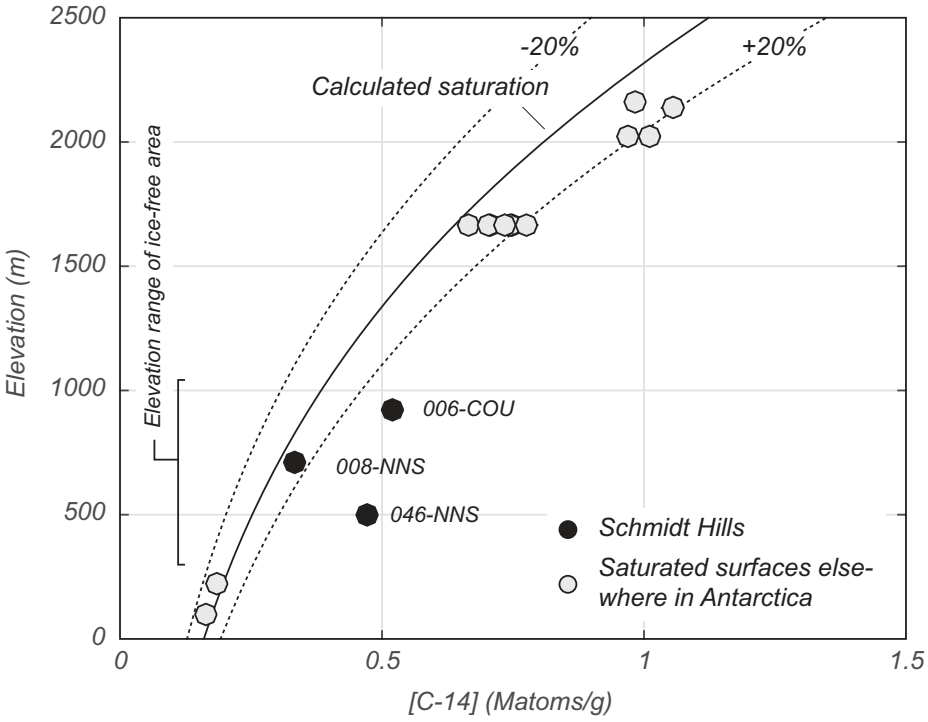

Fig. 13. Dark symbols show measured cosmogenic ^{14}C concentrations in quartz in Schmidt Hills erratics. Error bars (one standard error) are similar in size to symbols at this scale. The black line is the theoretical elevation - concentration relationship for production-decay saturation according to the "St" production rate scaling scheme of Balco and others (2008) with the Antarctic pressure-elevation model of Stone (2000). The light-colored symbols are measured ^{14}C concentrations in other Antarctic surfaces that are independently known to have been ice-free for more than 30 ka (Borchers and others, 2015).

atmosphere model of Stone (2000), and the production rate calibration data set described above, as well as (ii) existing measurements of ^{14}C concentrations in Antarctic bedrock surfaces that are independently known to have been ice-free for more than 30 ka. All three samples from the Schmidt Hills are at or above saturation concentrations at their respective elevations. Previous measurements of ^{14}C concentrations in ^{14}C-saturated surfaces elsewhere in Antarctica show some scatter as well as a systematic disagreement with calculations at high elevation; this is most likely the result of both unquantified analytical scatter and unrecognized systematic errors in production rate scaling or air pressure estimation. However, although these existing data lie within 20 percent of calculated saturation concentrations, two of our new measurements from the Schmidt Hills (10-MPS-006-COU and 10-MPS-046-NNS) are significantly higher than this range even in light of measurement and scaling uncertainties. A third measurement (10-MPS-008-NNS) is consistent with the expected saturation concentration at this site.

The only possible explanations for observed concentrations that are significantly higher than saturation are (i) unrecognized measurement error, and (ii) a theoretical scenario in which these samples spent a significant fraction of their recent exposure history at a much higher elevation and were very recently transported to their present locations. For example, the highest mountain summits in the Neptune Range to the southeast of the Schmidt Hills are 1600 to 1700 m elevation. The data and calculations

in figure 13 imply that saturated samples at 1600 to 1700 m have ^{14}C concentrations near 0.75 Matoms g^{-1}. If a ^{14}C-saturated sample from 1650 m elevation had been instantaneously transported to 900 m elevation at 7 ka, its present ^{14}C concentration would be 0.52 Matoms g^{-1}, similar to that observed in 10-MPS-006-COU. Likewise, the observed ^{14}C concentration in 10-MPS-046-NNS could be explained if the sample had been instantaneously transported from 1650 m elevation to 500 m elevation at 7 ka. These calculations show that it is theoretically possible to explain observed ^{14}C concentrations if glacier ice covering the Schmidt Hills during the middle Holocene transported previously exposed erratics from summit elevation to their present locations. However, other factors indicate that this scenario is unlikely. First, sample 10-MPS-046-NNS is granite, which does not outcrop anywhere in the Neptune Range (Schmidt and others, 1978). Granite erratics are extremely rare (we only collected one in this study) and have only been observed in glacial drift at relatively low elevations. Second, it is unlikely that erratics in the Schmidt Hills would be predominantly sourced from the tiny fraction of the ice-free portion of the Neptune Range that lies near summit elevations; the majority of ice-free areas lie at similar elevations to the Schmidt Hills, and the scenario described above is only feasible if there is a large elevation difference between the initial and present location of an erratic. On the other hand, if we reject this scenario, the only remaining explanation for ^{14}C concentrations exceeding saturation is unrecognized analytical error at least at the *ca.* 25 percent level, which is difficult to explain by known potential sources of error.

To summarize, if we exclude the possibility of unrecognized analytical errors, observed ^{14}C concentrations in Schmidt Hills erratics are only compatible with LGM ice cover of the Schmidt Hills under a complex and unlikely scenario in which these erratics were rapidly transported from a few specific mountain summits in the Neptune Range to their present locations in the Schmidt Hills during the middle to late Holocene. If we reject this scenario as well, the observation that ^{14}C concentrations are at or above production-decay saturation would provide strong evidence that the portion of the Schmidt Hills above 500 m was not covered by ice at the LGM. This issue could be resolved by replicate measurements aimed at eliminating the possibility of unrecognized analytical error. Regardless of this issue, however, although both geomorphic observations and geochemical data show that the Schmidt Hills have been covered by ice at some time in the past, there is no positive evidence that ice has been thicker than present at the Schmidt Hills during the LGM or Holocene.

Thomas Hills

We began analysis of Thomas Hills samples by measuring ^{3}He in quartz in nearly all samples collected (n = 109; figs. 14, 15 and 16). Apparent ^{3}He exposure ages were mainly in the 2 to 10 ka range, with a few as old as 100 ka. This distribution lies somewhere between those we observed at the Williams Hills (nearly all less than 5 ka) and the Schmidt Hills (nearly all greater than 5 ka). Again, at several sites we selected samples with the youngest apparent ^{3}He exposure ages for ^{10}Be measurements.

Two samples from the active ice-cored moraine at Clapperton Ridge (figs. 6 and 15) had apparent ^{10}Be ages less than 1 ka, which is consistent with the hypothesis that this moraine is actively forming at present. All other samples from the northern and central Thomas Hills had apparent ^{10}Be exposure ages between *ca.* 25 ka and *ca.* 1 Ma (fig. 15). Samples at Clapperton Ridge between 500 to 560 m and at Sugden Ridge are from landforms that belong to the Thomas Hills younger drift; apparent ^{10}Be exposure ages from both of these sites scatter in the range 20 to 40 ka (fig. 15). Samples above this level at Clapperton Ridge and Sugden Ridge as well as on the Mt. Warnke massif are older, ranging from 60 ka to 1 Ma.

Samples from the southern Thomas Hills (sites SML, SIS; figs. 6 and 16) have significantly younger apparent ^{10}Be exposure ages; approximately half lie in the range

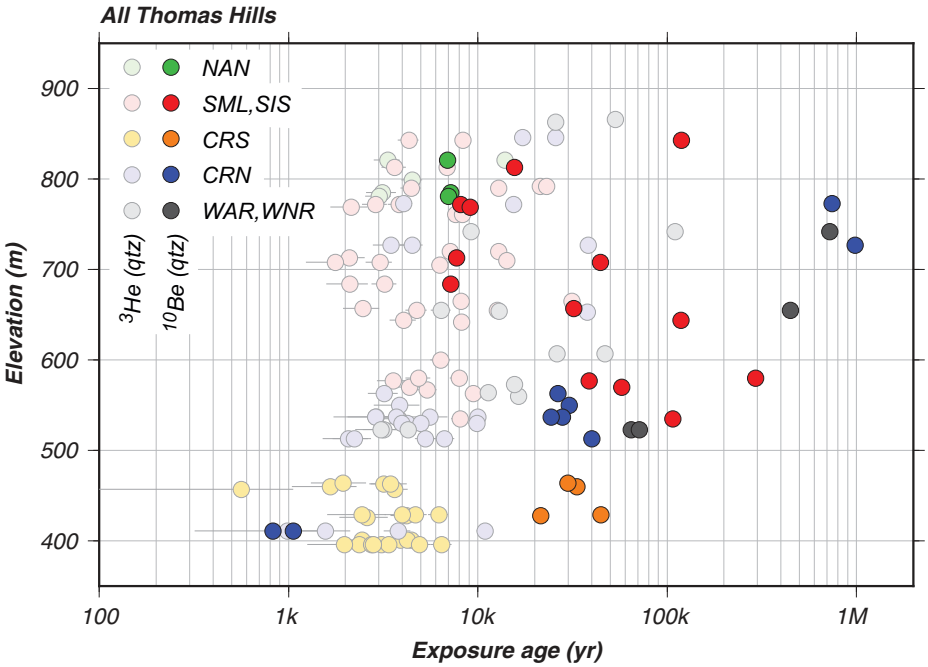

Fig. 14. Apparent ^{3}He-in-quartz and ^{10}Be-in-quartz exposure ages for all samples collected in the Thomas Hills. Colors correspond to named sample sites shown on figure 6. Some samples have multiple ^{3}He measurements, in which case each is shown as a distinct symbol. Error bars are one standard error. As the purpose of this figure is to compare multiple exposure ages from the same location, only measurement uncertainties are shown.

7 to 9 ka. The early Holocene cluster at South Mainland (SML; fig. 16) shows a positive correlation between age and elevation; those at Nance Ridge (NAN; fig. 16) are clustered in age and lie at approximately the same elevation.

In addition to the ^{3}He and ^{10}Be results shown in figures 14, 15 and 16, we measured ^{21}Ne in five boulders on Mt. Yarborough (fig. 6). In contrast to most of the samples that we collected from elevations above the Thomas Hills younger drift, which were erratic clasts perched on bedrock or colluvial substrates, these boulders were embedded in the Thomas Hills older till. Table 3 shows results. When corrected for nucleogenic ^{21}Ne as described above for the Schmidt Hills samples, apparent exposure ages are 1.2 to 2.4 Ma.

For the Thomas Hills, we conclude the following. First, a cluster of tightly grouped ^{10}Be ages between 7 and 9 ka at two sites in the southern Thomas Hills indicates that the LGM ice surface elevation was above 775 m elevation at South Mainland and 820 m elevation at Nance Ridge. Because we observe older ^{10}Be ages both above and below this level at South Mainland, it is unclear whether the cluster of samples with ages 7 to 9 ka represent the LGM ice limit in the Thomas Hills or not. In any case, we interpret these samples to record early to middle Holocene ice sheet thinning at these sites. This is consistent with the ^{10}Be results from the Williams Hills. Other samples with older exposure ages at South Mainland presumably record repeated cover of this site by frozen-based ice, as expected from geomorphic observations, in particular the presence of erratics with a wide range of weathering states.

In contrast, evidence for LGM or Holocene ice cover of the north-central Thomas Hills is absent. Deposits of Thomas Hills younger drift with apparent exposure ages 20

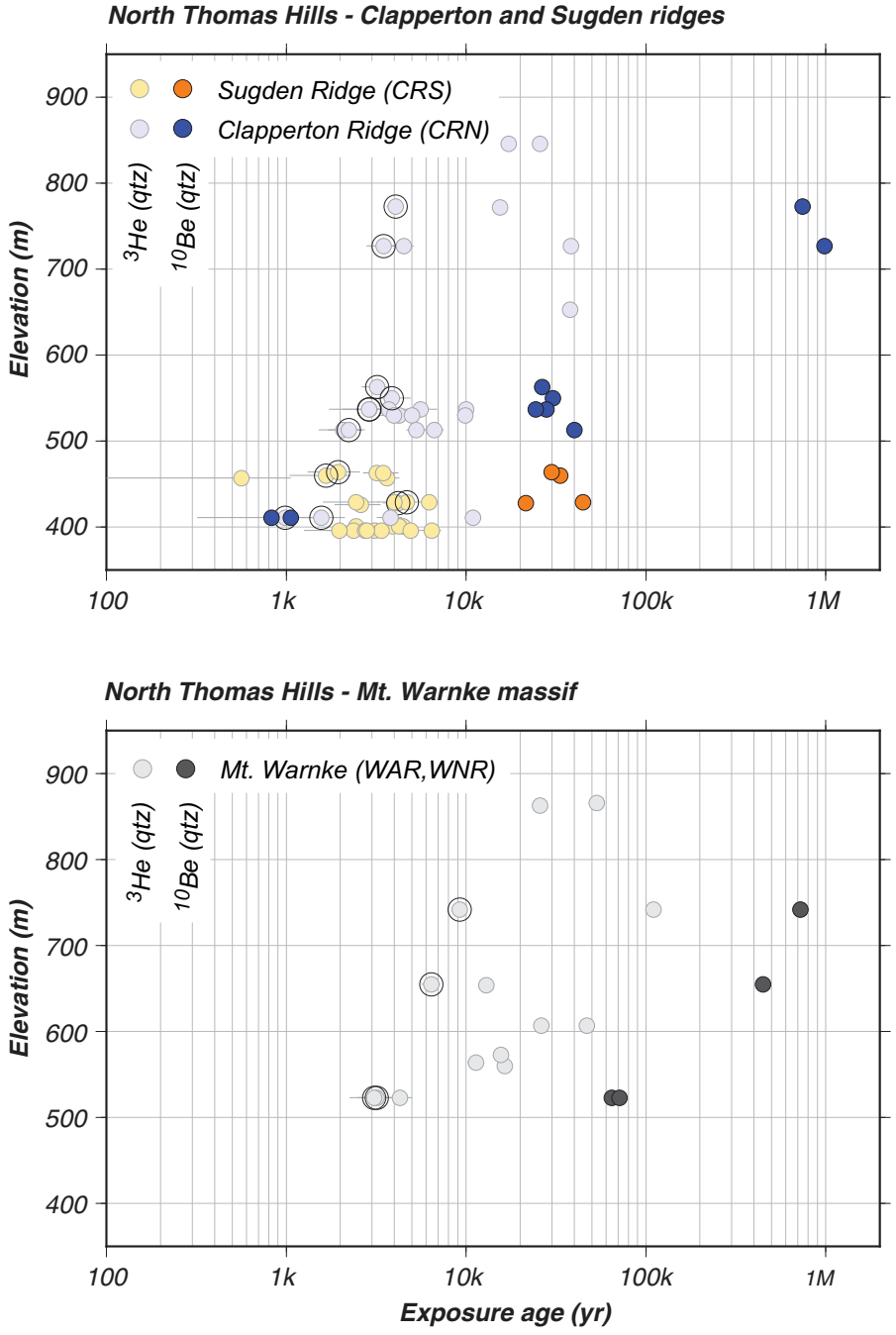

Fig. 15. Apparent ^{3}He-in-quartz and ^{10}Be-in-quartz exposure ages for sites in the north-central Thomas Hills. Colors correspond to named sample sites shown on figure 6. Both plots show subsets of the data shown on figure 14. In both panels, dark circles around ^{3}He data indicate the samples for which we also measured ^{10}Be concentrations.

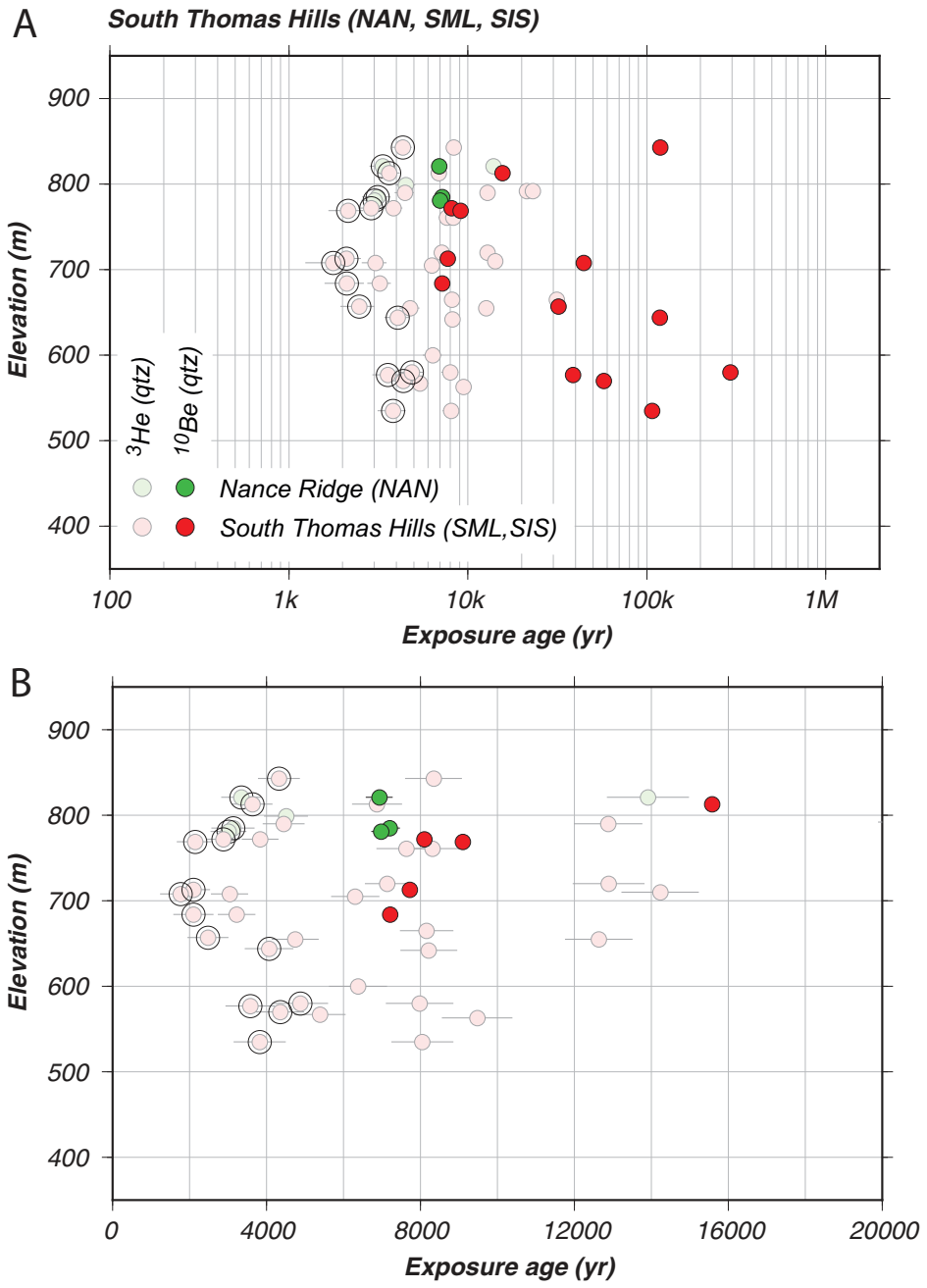

Fig. 16. Apparent ^{3}He-in-quartz and ^{10}Be-in-quartz exposure ages for the southern Thomas Hills. Colors correspond to named sample sites shown on figure 6. (A) and (B) panels show the same data on different x-axes; both show subsets of the data shown on figure 14. In both panels, dark circles around ^{3}He data indicate the samples for which we also measured ^{10}Be concentrations.

TABLE 3

^{21}Ne exposure ages for boulders associated with the Thomas Hills older till at Mt. Yarborough

Sample name	aliquot	$[^{21}Ne]_{xs}$ (measured) (Matoms g^{-1})	+/-	$[^{21}Ne]_c$ (calculated) (Matoms g^{-1})	+/-	Apparent exposure age (Ma)
11-ATH-310-YAR	a	118.70	3.76	106.5	5.1	2.40 +/- 0.12 (0.16)
11-ATH-311-YAR	a	76.37	3.91	64.1	5.2	1.47 +/- 0.12 (0.14)
11-ATH-313-YAR	a	88.18	3.39	75.9	4.8	
11-ATH-313-YAR	b	85.59	3.19	73.3	4.7	
		Error-weighted mean		74.6	3.4	1.762 +/- 0.080 (0.117)
11-ATH-314-YAR	a	90.47	3.09	78.2	4.6	1.85 +/- 0.11 (0.14)
11-ATH-315-YAR	a	62.04	2.97	49.8	4.5	
11-ATH-315-YAR	b	65.58	3.19	53.3	4.7	
		Error-weighted mean		51.5	3.2	1.217 +/- 0.076 (0.096)

to 40 ka at elevations below 560 m, taken by themselves, would indicate that (i) this drift records the most recent period of glacier thickening at this site, and (ii) this event took place well before the generally recognized LGM in Antarctica. However, the evidence for LGM ice cover and Holocene deglaciation in the southern Thomas Hills at elevations up to 820 m would, presumably, imply that the younger drift at 560 m elevation in the central Thomas Hills was also ice-covered at this time, in which case apparent exposure ages for the younger Thomas Hills drift would provide only a minimum age for the drift. For the central Thomas Hills to have remained ice-free since 20 to 40 ka while ice was nearly 300 m thicker in the southern Thomas Hills in the early Holocene would require extremely steep ice surface slopes, which, although not impossible given the relatively steep ice surface topography in the vicinity of the Thomas Hills at present, appears unlikely.

Finally, exposure ages from boulders belonging to the Thomas Hills older till at Mt. Yarborough are most likely minimum ages in light of evidence for boulder weathering, possible exhumation from till, and possible postdepositional ice cover of these sites. Thus, they imply that the older till was emplaced before 2.4 Ma.

Cosmogenic ^{3}He Diffusion in Quartz

In this work we collected an unusually large set of paired ^{3}He and ^{10}Be measurements from quartz samples. Here we discuss this data set from the perspective of, first, the usefulness of using ^{3}He measurements as a means of efficiently screening exposure-dating samples for prior exposure, and, second, whether we can gain any insight into He diffusion kinetics in quartz from these data.

Figure 17 shows apparent ^{3}He and ^{10}Be exposure ages computed for all samples where both nuclides were measured, compared to model calculations of ^{3}He retention during continuous surface exposure. The premise of using ^{3}He concentrations in quartz as a rapid screening method to identify pre-exposed erratics is that even though the apparent ^{3}He exposure age will always underestimate the true exposure age of a sample due to diffusive loss of ^{3}He, at least the apparent ^{3}He age will be a monotonic function of the true age. In other words, apparent ^{3}He exposure ages of samples with pre-LGM ^{10}Be ages will be greater than apparent ^{3}He exposure ages of samples with

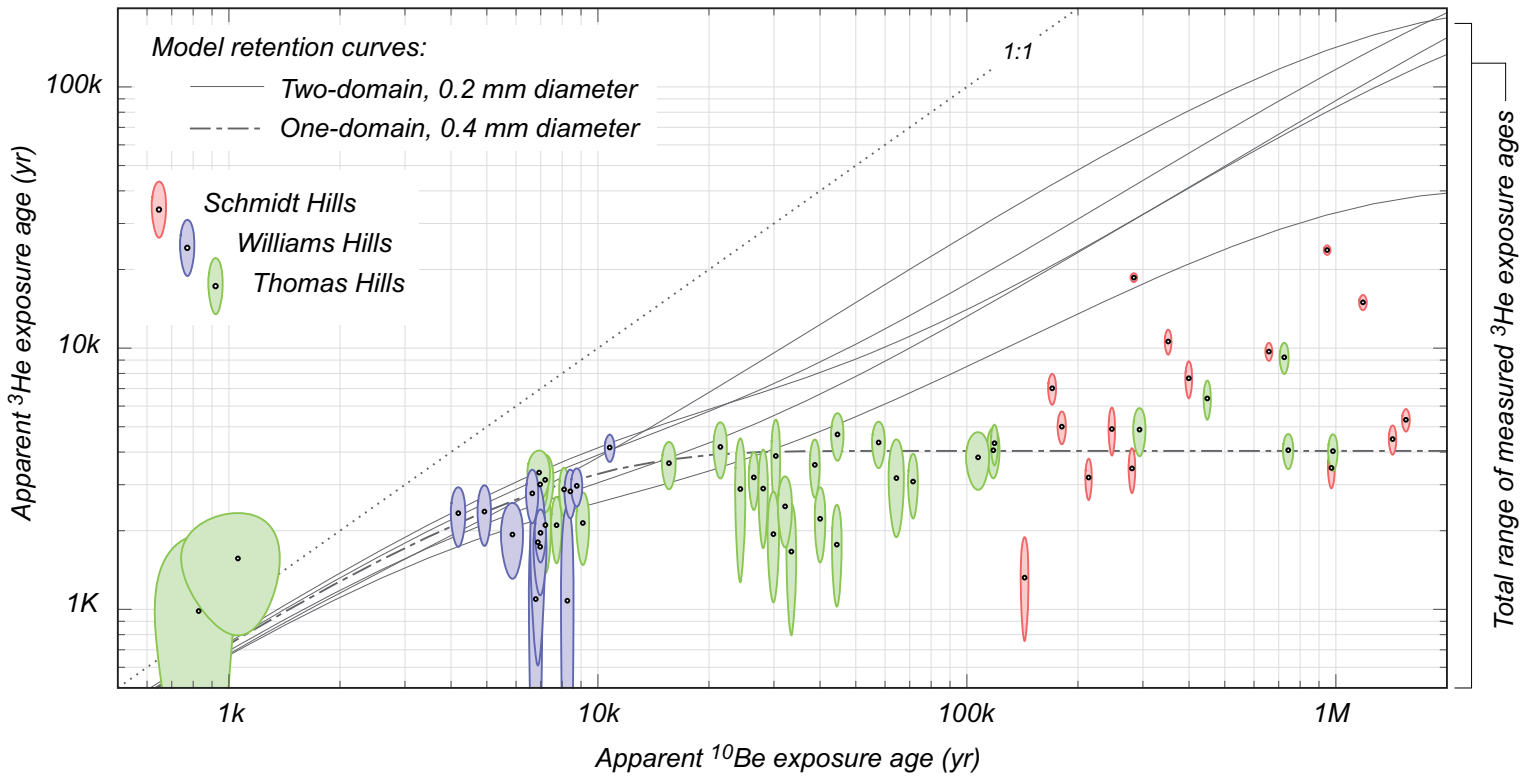

Fig. 17 Apparent ^{3}He and ^{10}Be exposure ages in samples where both were measured. Ellipses are 68% confidence regions including measurement uncertainty only. Dark lines that lie below the 1:1 line are model isothermal retention curves computed for continuous surface exposure, with a variety of estimates for He diffusion kinetics in quartz (see text for discussion).

Holocene ^{10}Be ages. Figure 17 shows that this is not generally true for our data set. Instead, samples with apparent ^{3}He-in-quartz exposure ages in the 2 to 5 ka range have ^{10}Be exposure ages ranging from 4 ka to greater than 1 Ma. Thus, our screening method was effective in identifying and excluding from ^{10}Be analysis a number of samples with apparent ^{3}He exposure ages older than *ca.* 25 ka that could not under any circumstances have LGM-to-Holocene true exposure ages. However, it was not effective in selecting samples emplaced after the LGM from among the population of samples with young apparent ^{3}He exposure ages. In this section, we investigate this issue by considering diffusion kinetics of ^{3}He in quartz in more detail.

In general, diffusive loss of noble gases from minerals depends on the material properties of the mineral itself (the "diffusion kinetics"), the ambient temperature, and the size of the mineral grain (for example, Baxter, 2010). Shuster and Farley (2005) experimentally determined He diffusion kinetics in a sample of gem-quality quartz and found that their observations could be explained if quartz grains behaved as a single diffusion domain in which diffusivity obeys a simple Arrhenius relationship to temperature, as is commonly the case for many minerals. However, Tremblay and others (2014b) performed similar measurements on many natural quartz samples and found that some samples displayed more complex behavior that was inconsistent with a single-domain model, but consistent with a two-domain model in which ^{3}He in quartz is hosted in two separate domains with distinct Arrhenius parameters. One- and two-domain models with kinetic parameters estimated from these experiments imply significantly different predictions for cosmogenic ^{3}He retention in quartz. A single-domain model with the kinetic parameters of Shuster and Farley (2005) predicts that the cosmogenic ^{3}He concentration in quartz grains will reach equilibrium between production and diffusive loss in thousands to tens of thousands of years for grain sizes commonly analyzed ($<$ 1 mm) and typical Antarctic temperatures. However, two-domain models with kinetic parameters from Tremblay and others (2014b) predict, for the same grain size and temperature, that the higher-retentivity domain may require more than 1 Myr to reach production-diffusion equilibrium. This difference is important from the perspective of using ^{3}He measurements to screen for pre-exposure, because the single-domain model predicts that samples whose true exposure age exceeds the time required to reach production-diffusion steady state will all display the same apparent ^{3}He exposure age. In this case, for the grain size-temperature range applicable to this study and many similar studies in Antarctica, ^{3}He concentrations in erratics emplaced before and after the LGM could be the same. The two-domain models, on the other hand, predict a monotonic, although nonlinear, relation between apparent ^{3}He age and true age up to ages much older than the LGM. In this latter case it would generally be possible to distinguish between erratics emplaced after the LGM and those emplaced earlier.

Figure 17 illustrates this with model ^{3}He retention curves generated as follows. First, a retention curve represents the evolution of ^{10}Be and ^{3}He concentrations during a single period of uninterrupted surface exposure, so in figure 17 the apparent ^{10}Be exposure age on the x-axis is considered the true exposure age for the purposes of comparing observations to the retention curves. Note that ^{10}Be and ^{3}He concentrations in samples that have experienced episodic burial under ice, as is likely for many of our samples, would not lie on retention curves constructed in this way. Second, we assumed an effective diffusion temperature for the sample sites of -16 °C (the effective diffusion temperature is higher than the mean annual temperature when daily and seasonal temperature variability is present, because diffusivity is nonlinear with respect to temperature; see discussion in Tremblay and others, 2014a). Third, we assumed, based on the discussion earlier in this paper, that samples with Holocene ^{10}Be exposure ages from the Williams and Thomas Hills have, in fact, experienced a

single period of uninterrupted surface exposure, so ^{10}Be and ^{3}He concentrations in those samples should lie on model retention curves. Thus, we forced retention curves to pass through these data by adjusting the effective grain size used in the model calculations. In principle it would be possible to estimate the effective grain size independently by direct measurement. In this case, however, although samples for ^{3}He analysis were sieved to a consistent grain size fraction after crushing, we did not systematically carry out thin section analysis needed to accurately determine the natural size of quartz grains in sandstone erratics prior to crushing. Model retention curves drawn through the Holocene data imply that the effective grain size of these samples (0.2–0.4 mm) is likely less than the sieve size used to prepare aliquots for analysis (0.25–0.85 mm). That is, many of the grains we analyzed were probably aggregates of smaller grains. This is not surprising for relatively poorly sorted and weakly metamorphosed sandstones.

We then calculated model retention curves as described by Wolf and others (1998), using two kinetic models. The dashed line in figure 17 shows ^{3}He retention predicted by a single-domain model and the kinetic parameters of Shuster and Farley (2005). The four solid lines show ^{3}He retention predicted by a two-domain model fit to laboratory data for four sandstone erratics from the Williams Hills using the experimental method and fitting procedure of Tremblay and others (2014b); results from these samples cannot be fit with a one-domain model (M. Tremblay, unpublished dissertation research). A single-domain model that accurately estimates ^{3}He concentrations in Holocene erratics predicts production-diffusion steady-state for ^{3}He after *ca.* 20 ka of continuous exposure, whereas two-domain models that also fit the data from Holocene erratics predict steady state only after more than 1 Ma, and permit much higher possible range of ^{3}He concentrations.

Figure 17 shows that although nearly all samples are sandstone erratics with similar lithology to those at the Williams Hills, observed ^{3}He retention in many samples with old ^{10}Be exposure ages is widely scattered with respect to any one of the kinetic models that fit the Holocene data. In other words, any of the kinetic models can be tuned to fit the Holocene data or some fraction of the older data, but not all the data.

There are several possible explanations for this failure of any model retention curve to adequately explain a significant fraction of the observations. Many of these explanations are untenable, for example the possibility of large variations in effective temperature among samples that lie on the same outcrop. One possible explanation relates to repeated burial of pre-LGM samples by ice. During periods of ice cover, production of ^{3}He will cease, but diffusive loss will continue; thus, samples that have been covered by ice for a long time will have ^{3}He/^{10}Be ratios that are lower than otherwise identical samples that have not been covered by ice. This effect is closely analogous to the effect of repeated exposure and ice cover on ^{26}Al/^{10}Be ratios in quartz (for example, Lal, 1991; Balco and others, 2014 and references therein), although it would be more sensitive to short periods of ice cover because diffusive loss of ^{3}He is generally faster than radioactive decay of ^{26}Al. Thus, it is possible that the two-domain kinetic models accurately describe He diffusion kinetics in Pensacola Mountains quartz, and the difference between observed ^{3}He concentrations and those predicted by ^{10}Be ages and model retention curves shows that these samples have experienced long periods of burial by ice. Although we have not done this in the present study, this hypothesis could be tested by comparing ^{3}He retention to, for example, ^{26}Al/^{10}Be ratios in samples with old apparent ^{10}Be exposure ages.

A second potential reason for this disagreement between observed ^{3}He retention and any particular model retention curve is simply that quartz diffusion kinetics are highly variable among samples. Although no single model retention curve explains all of our observations, the observed variation in ^{3}He retention in samples with pre-

Holocene exposure ages is similar to the variation among model retention curves computed for end-member one- and two-domain diffusion kinetics. In other words, if we rejected the possibility of episodic burial and assumed that all samples had experienced continuous exposure, observed ^{3}He retention for nearly all samples would lie within the range predicted by end member kinetic models. Although the majority of the erratic samples we analyzed were medium- to coarse-grained sandstones of similar lithology, the potential variation in quartz provenance inherent to sedimentary rocks would be consistent with the idea that we may have sampled a significant fraction of the full range of diffusion kinetics observed in natural quartz samples (Tremblay and others, 2014b). This possibility is important because the goal of applying a screening approach, in which we selected samples with the lowest apparent ^{3}He exposure ages for ^{10}Be measurements, was to identify the samples with the lowest true exposure ages. If the range of ^{3}He retention we observe is in fact the result of inter-sample variability in diffusion kinetics, then we would not necessarily have identified the samples with the lowest true exposure ages, but instead identified the samples with the least retentive diffusion kinetics regardless of their exposure age. This suggests that the ^{3}He-in-quartz screening method would probably be more effective for erratics of a single igneous or metamorphic lithology, where it is more likely that quartz from all samples will share common diffusion kinetics.

conclusions: lgm-to-present ice thickness changes

The ^{10}Be exposure-age data from the Williams Hills show that surrounding ice, presumably including the FIS and Academy Glacier, was more than 500 m thicker prior to 10 ka. Ice thinning took place between 11 ka and 5 ka at an average rate of approximately 9 cm yr^{-1}. The exposure-age data indicate steady thinning during the period, although they are not spaced closely enough in elevation to exclude the possibility of rapid thinning events at the scale of tens of meters and hundreds of years.

Exposure-age data from the southern Thomas Hills are consistent with observations from the Williams Hills and imply that ice surrounding the Thomas Hills was at least 400 m thicker prior to *ca.* 9 ka and thinned to its present configuration during the Holocene. Although in the Thomas Hills we only found erratics with LGM-to-Holocene exposure ages at the south end of the range, these observations would most likely require that the entire Thomas Hills massif was similarly covered by thicker ice, unless local ice surface slopes were significantly steeper than observed at present (fig. 18). As the geomorphology of all sites we visited in this study is consistent with repeated episodes of cover by frozen-based ice, we conclude that the majority of samples we collected in the Thomas Hills, including samples from the Thomas Hills younger drift, were covered by ice at the LGM, and apparent exposure ages of these samples underestimate the true emplacement ages of the underlying deposits.

With the exception of clasts from the actively forming moraine at the present ice margin in the Thomas Hills, we did not observe any exposure ages younger than 4 ka. Thus, our observations are consistent with the hypothesis that grounding lines of glaciers and ice streams flowing into the Weddell Sea were farther inland than present during the middle to late Holocene and have advanced during the late Holocene (for example, Bradley and others, 2015). In this scenario, ice in our study area would most likely have been thinner than present during the late Holocene, so any geologic record of late Holocene events would be buried beneath the present ice surface. However, exposure-age data from the Williams Hills do constrain any late Holocene ice thickness minimum to have occurred after 4 ka.

In contrast to the Williams and Thomas Hills, there is no evidence for thicker ice during the LGM or Holocene at the Schmidt Hills. In fact, ^{14}C measurements appear to provide evidence that the LGM ice thickness was less than *ca.* 200 m greater than present. It is difficult to reconcile substantial thickening at the Williams Hills with zero

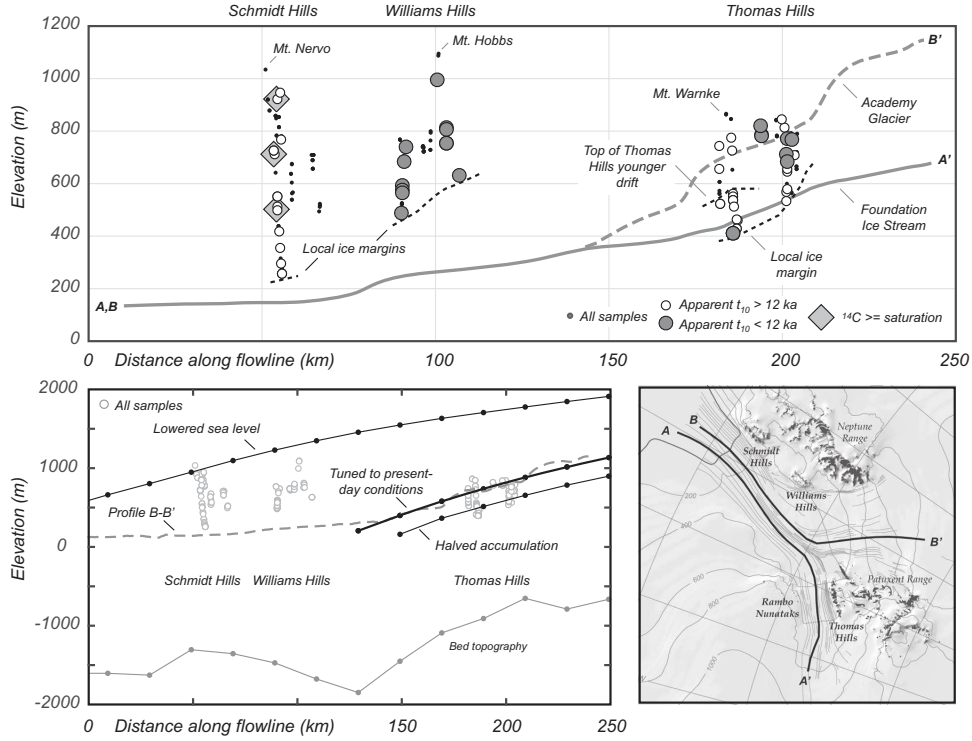

Fig. 18. Exposure-age results projected onto elevation profile along flowlines of Foundation Ice Stream and Academy Glacier; lower right panel shows profile locations. Elevation data are from the 2009 ERS/Icesat DEM (Bamber and others, 2009). Sample locations are projected to nearest point on profile A-A'. In the upper panel, symbols denote locations of samples that were (i) collected but not analyzed for ^{10}Be (small black circles); (ii) collected and analyzed for ^{10}Be (larger circles); and (iii) analyzed for ^{14}C (diamonds). The distribution of sample locations approximates the extent of ice-free areas on the nunataks where samples were collected. Lines marked "local ice margin" show the elevation of the lowermost ice-free areas on major nunataks and are highly simplified for purposes of this figure; in reality the shape of the ice margin is more complex (see figs. 2, 3, 4, 6, and 7). Overall, the present ice margin is significantly higher than the FIS at the Schmidt and Williams Hills, and close to or lower than the FIS at the Thomas Hills. The panel at lower left shows results of numerical model experiments as well as prescribed bed topography for the Academy Glacier flowband (coincident with profile B-B') from Huybers (ms, 2014); dots show model mesh points. The model result marked 'present-day conditions' has modern boundary conditions and is tuned to match the present ice surface elevation. The result marked 'lowered sea level' is the endpoint of a 15,000-year transient model run with the same boundary conditions but relative sea level lowering of 100 m; the model response to this forcing is unstable grounding line advance to the edge of the model domain on the continental shelf. The "halved accumulation' result has the same boundary conditions as the modern simulation except that the accumulation rate is halved in the entire model domain.

thickening at the Schmidt Hills, because ice could only be both (i) more than 500 m thicker than present at the Williams Hills and (ii) less than 200 m thicker than present at the Schmidt Hills if the surface slope of the FIS near the present grounding zone was significantly greater than present. This, in turn, is glaciologically unlikely because the most likely mechanism for LGM thickening of the FIS would be grounding line advance due to lowered relative sea level, which would result in both thicker ice at the Schmidt Hills and a shallower ice surface slope in the vicinity of the Schmidt and Williams Hills. Figure 18 illustrates this point with results of numerical flowband model simulations for the FIS-Academy Glacier from Huybers (ms, 2014). Model runs forced by relative sea level lowering that predict grounding line advance onto the continental shelf display a shallower ice surface slope in the Schmidt Hills - Williams Hills region,

which is inconsistent with the interpretation that the Williams Hills were ice-covered at the LGM but the Schmidt Hills were not. In contrast, model runs in which the grounding line does not advance and the LGM accumulation rate is lower than present predict lower ice surface elevations at all sites, which is also inconsistent with the observations.

Overall, figure 18 highlights the following points. One, the magnitude of LGM-to-Holocene ice thickness change inferred from the distribution of Holocene exposure ages is consistent between the Williams and Thomas Hills. Two, if the Holocene exposure ages from the Williams Hills and southern Thomas Hills record LGM/Holocene ice cover, then it is most likely that Thomas Hills younger drift was also ice covered at the LGM. Three, a very steep ice surface slope in the vicinity of the present grounding zone is required to reconcile 500 m thicker ice in the early Holocene in the Williams Hills with the absence of any LGM-to-present ice cover at the sites of ^{14}C measurements in the Schmidt Hills.

We see two possible scenarios that would reconcile observations from the Schmidt and Williams Hills. First, it is possible that our ^{14}C measurements are in error for some reason that we have not identified, and the Schmidt Hills were covered by significantly thicker frozen-based ice, that deposited no drift or left any geologic evidence of its presence, during the LGM and early Holocene. This would be consistent with the fact that the Schmidt Hills are a local accumulation area at present; if this was also the case during the LGM, ice flow away from the hills toward the FIS might preclude emplacement of erratics derived from elsewhere. On the other hand, although the Williams Hills are a local accumulation area currently, many Holocene erratics are present. In any case, this scenario could be most easily evaluated by independently replicating the ^{14}C measurements.

A second, more complex, scenario would accept the ^{14}C measurements but take note of the fact that, at present, the Schmidt Hills form a local accumulation area and the ice margin lies at least 100 m above the present surface of the FIS, whereas the Thomas Hills are a local ablation area and the ice margin is up to 75 m below the present FIS surface. If during the LGM the Schmidt Hills were an ablation area as the Thomas Hills are today, and the local ice margin was likewise 75 m below the FIS surface elevation, then the FIS could potentially have been up to *ca.* 350 m thicker in the vicinity of the Schmidt Hills without covering the site of our lowest ^{14}C measurement. In this scenario, LGM-to-present thinning of the FIS would be simultaneous with growth and thickening of locally fed glaciers and icefields surrounding the Schmidt Hills, and geologic evidence of the LGM and early Holocene ice margin configuration would be buried by ice at present. Although the existence of a widespread unconformity beneath locally derived ice in the Schmidt Hills imaged by ice-penetrating radar (Campbell and others, 2013) might support this hypothesis, it is unclear what other geological or geochronological data could be used to unambiguously test it. In part it could be evaluated with ^{14}C measurements on samples near the present ice margin at the Schmidt Hills.

To summarize, although exposure-age data clearly indicate that the FIS was more than 500 m thicker during the early Holocene at the Williams Hills and Thomas Hills, available data appear inconsistent with LGM or early Holocene thickening in excess of *ca.* 200 m at the Schmidt Hills. These observations are difficult to reconcile with each other. Overall, observations from the Schmidt Hills appear inconsistent with a scenario in which the LGM grounding line of the FIS was located on the outer continental shelf, whereas observations from the Williams and Thomas Hills appear inconsistent with a scenario in which the FIS grounding line remained near its present position at the LGM.

ACKNOWLEDGMENTS

Funding for this work was provided by the U.S. National Science Foundation via grants PLR-0838783, PLR-0838784, and PLR-0838256, and by the Ann and Gordon Getty Foundation. We thank Chris Simmons for field mountaineering support; pilots, crews, and ground staff of the 109th Airlift Wing of the New York Air National Guard and Kenn Borek Air, Ltd. for air support; McMurdo Station staff and many other U.S. Antarctic Program personnel for logistical planning and execution; Tim Becker and David Shuster (BGC) for assistance with cosmogenic noble gas measurements; Susan Zimmerman (LLNL-CAMS) for assistance with AMS measurements; Nat Lifton, Marc Caffee, and Tom Kubley (PRIME Lab) for assistance with ^{14}C analyses; and Marissa Tremblay (UC Berkeley) for providing unpublished results of diffusion experiments on Williams Hills erratics. In addition, we thank Robert Ackert for a helpful and comprehensive review.

REFERENCES

Ackert, R. P., Jr., Mukhopadhyay, S., Parizek, B. R., and Borns, H. W., 2007, Ice elevation near the West Antarctic Ice Sheet divide during the last glaciation: Geophysical Research Letters, v. 34, n. 21, L21506, http://dx.doi.org/10.1029/2007GL031412

Balco, G., 2011, Contributions and unrealized potential contributions of cosmogenic-nuclide exposure dating to glacier chronology, 1990–2010: Quaternary Science Reviews, v. 30, n. 1–2, p. 3–27, http://dx.doi.org/10.1016/j.quascirev.2010.11.003

Balco, G., and Shuster, D. L., 2009a, Production rate of cosmogenic ^{21}Ne in quartz estimated from ^{10}Be, ^{26}Al, and ^{21}Ne concentrations in slowly eroding Antarctic bedrock surfaces: Earth and Planetary Science Letters, v. 281, n. 1–2, p. 48–58, http://dx.doi.org/10.1016/j.epsl.2009.02.006

——— 2009b, ^{26}Al-^{10}Be-^{21}Ne burial dating: Earth and Planetary Science Letters, v. 286, n. 3–4, p. 570–575, http://dx.doi.org/10.1016/j.epsl.2009.07.025

Balco, G., Stone, J. O., Lifton, N. A., and Dunai, T. J., 2008, A complete and easily accessible means of calculating surface exposure ages or erosion rates from ^{10}Be and ^{26}Al measurements: Quaternary Geochronology, v. 3, n. 3, p. 174–195, http://dx.doi.org/10.1016/j.quageo.2007.12.001

Balco, G., Briner, J., Finkel, R. C., Rayburn, J. A., Ridge, J. C., and Schaefer, J. M., 2009, Regional beryllium-10 production rate calibration for late-glacial northeastern North America: Quaternary Geochronology, v. 4, n. 2, p. 93–107, http://dx.doi.org/10.1016/j.quageo.2008.09.001

Balco, G., Shuster, D. L., Blard, P. H., Zimmermann, L., and Stone, J. O. H., 2011, Cosmogenic ^{21}Ne production systematics in quartz inferred from a 25-meter sandstone core: Mineralogical Magazine, v. 75, p. 473.

Balco, G., Schaefer, J. M., and LARISSA group, 2013, Exposure-age record of Holocene ice sheet and ice shelf change in the northeast Antarctic Peninsula: Quaternary Science Reviews, v. 59, p. 101–111, http://dx.doi.org/10.1016/j.quascirev.2012.10.022

Balco, G., Stone, J. O., Sliwinski, M. G., and Todd, C., 2014, Features of the glacial history of the Transantarctic Mountains inferred from cosmogenic ^{26}Al, ^{10}Be and ^{21}Ne concentrations in bedrock surfaces: Antarctic Science, v. 26, p. 708–723, http://dx.doi.org/10.1017/S0954102014000261

Bamber, J. L., Gomez-Dans, J. L, and Griggs, J. A., 2009, Antarctic 1 km Digital Elevation Model (DEM) from Combined ERS-1 Radar and ICESat Laser Satellite Altimetry: Boulder, Colorado, USA, National Snow and Ice Data Center, Digital media.

Baxter, E. F., 2010, Diffusion of noble gases in minerals: Reviews in Mineralogy and Geochemistry, v. 72, n. 1, p. 509–557, http://dx.doi.org/10.2138/rmg.2010.72.11

Bentley, M. J., Fogwill, C. J., Le Brocq, A. M., Hubbard, A. L., Sugden, D. E., Dunai, T. J., and Freeman, S. P. T., 2010, Deglacial history of the West Antarctic Ice Sheet in the Weddell Sea embayment: Constraints on past ice volume change: Geology, v. 38, n. 5, p. 411–414, http://dx.doi.org/10.1130/G30754.1

Blard, P. H., Balco, G., Burnard, P. G., Farley, K. A., Fenton, C. R., Friedrich, R., Jull, A. J. T., Niedermann, S., Pik, R., Schaefer, J. M., Scott, E. M., Shuster, D. L., Stuart, F. M., Stute, M., Tibari, B., Winkler, G., and Zimmermann, L., 2015, An inter-laboratory comparison of cosmogenic ^{3}He and radiogenic ^{4}He in the CRONUS-P pyroxene standard: Quaternary Geochronology, v. 26, p. 11–19, http://dx.doi.org/10.1016/j.quageo.2014.08.004

Borchers, B., Marrero, S., Balco, G., Caffee, M., Goehring, B., Lifton, N., Nishiizumi, K., Phillips, F., Schaefer, J., and Stone, J., 2015, Geological calibration of spallation production rates in the CRONUS-Earth Project: Quaternary Geochronology, v. 31, p. 188–198, http://dx.doi.org/10.1016/j.quageo.2015.01.009

Bradley, S. L., Hindmarsh, R. C., Whitehouse, P. L., Bentley, M. J., and King, M. A., 2015, Low post-glacial rebound rates in the Weddell Sea due to Late Holocene ice-sheet readvance: Earth and Planetary Science Letters, v. 413, p. 79–89, http://dx.doi.org/10.1016/j.epsl.2014.12.039

Brook, E. J., and Kurz, M. D., 1993, Surface-exposure chronology using *in situ* cosmogenic ^{3}He in Antarctic quartz sandstone boulders: Quaternary Research, v. 39, n. 1, p. 1–10, http://dx.doi.org/10.1006/qres.1993.1001

Campbell, S., Balco, G., Todd, C., Conway, H., Huybers, K., Simmons, C., and Vermeulen, M., 2013,

Radar-detected englacial stratigraphy in the Pensacola Mountains, Antarctica: implications for recent changes in ice flow and accumulation: Annals of Glaciology, v. 54, n. 63, p. 91–100, http://dx.doi.org/10.3189/2013AoG63A371

Fernandez-Mosquera, D., Marti, H., Hahm, D., Vidal-Romani, J., Braucher, R., and Bourlès, D., 2008, Muon produced neon in quartz at large depths: BeNe project progress report: Geochimica Et Cosmochimica Acta, v. 72, n. 12, Supplement, p. A265.

Graf, W., Reinwarth, O., Oerter, H., Mayer, C., and Lambrecht, A., 1999, Surface accumulation on foundation ice stream, Antarctica: Annals of Glaciology, v. 29, n. 1, p. 23–28, http://dx.doi.org/10.3189/172756499781820987

Heisinger, B., Lal, D., Jull, A. J. T., Kubik, P., Ivy-Ochs, S., Neumaier, S., Knie, K., Lazarev, V., and Nolte, E., 2002a, Production of selected cosmogenic radionuclides by muons: 1. Fast muons: Earth and Planetary Science Letters, v. 200, n. 3–4, p. 345–355, http://dx.doi.org/10.1016/S0012-821X(02)00640-4

Heisinger, B., Lal, D., Jull, A. J. T., Kubik, P., Ivy-Ochs, S., Knie, K., and Nolte, E., 2002b, Production of selected cosmogenic radionuclides by muons: 2. Capture of negative muons: Earth and Planetary Science Letters, v. 200, n. 3–4, p. 357–369, http://dx.doi.org/10.1016/S0012-821X(02)00641-6

Heyman, J., 2014, Paleoglaciation of the Tibetan Plateau and surrounding mountains based on exposure ages and ELA depression estimates: Quaternary Science Reviews, v. 91, p. 30–41, http://dx.doi.org/10.1016/j.quascirev.2014.03.018

Hillenbrand, C. D., Bentley, M. J., Stolldorf, T. D., Hein, A. S., Kuhn, G., Graham, A. G., Fogwill, C. J., Kristoffersen, Y., Smith, J. A., Anderson, J. B., Larter, R. D., Melles, M., Hodgson, D. A., Mulvaney, R., and Sugden, D. E., 2014, Reconstruction of changes in the Weddell Sea sector of the Antarctic Ice Sheet since the Last Glacial Maximum: Quaternary Science Reviews, v. 100, p. 111–136, http://dx.doi.org/10.1016/j.quascirev.2013.07.020

Hippe, K., and Lifton, N. A., 2014, Calculating isotope ratios and nuclide concentrations for *In situ* cosmogenic ^{14}C analyses: Radiocarbon, v. 56, n. 3, p. 1167–1174, http://dx.doi.org/10.2458/56.17917

Huybers, K. M., ms, 2014, Relationships between Climate and Geophysical Processes : What Climate Histories Can Be Inferred from Glaciers, Lakes, and Ice Streams?: Seattle, Washington, University of Washington, Ph. D. thesis, 166 p., available online: https://digital.lib.washington.edu/researchworks/handle/1773/26276

Kaplan, M. R., Strelin, J. A., Schaefer, J. M., Denton, G. H., Finkel, R. C., Schwartz, R., Putnam, A. E., Vandergoes, M. J., Goehring, B. M., and Travis, S. G., 2011, *In-situ* cosmogenic ^{10}Be production rate at Lago Argentino, Patagonia: Implications for late-glacial climate chronology: Earth and Planetary Science Letters, v. 309, n. 1–2, p. 21–32, http://dx.doi.org/10.1016/j.epsl.2011.06.018

Lal, D., 1991, Cosmic ray labeling of erosion surfaces: *In situ* nuclide production rates and erosion models: Earth and Planetary Science Letters, v. 104, n. 2–4, p. 424–439, http://dx.doi.org/10.1016/0012-821X(91)90220-C

Lifton, N., Goehring, B., Wilson, J., Kubley, T., and Caffee, M., 2015, Progress in automated extraction and purification of *in situ* ^{14}C from quartz: Results from the Purdue *in situ* ^{14}C laboratory: Nuclear Instruments and Methods in Physics Research Section B: Beam Interactions with Materials and Atoms, v. 361, p. 381–386, http://dx.doi.org/10.1016/j.nimb.2015.03.028

Liu, H., Jezek, K., Li, B., and Zhao, Z., 2001, Radarsat Antarctic Mapping Project Digital Elevation Model Version 2. . Boulder, Colorado, USA: National Snow and Ice Data Center, http://dx.doi.org/10.5067/PXKC81A7WAXD.

Middleton, J. L., Ackert, R. P., Jr., and Mukhopadhyay, S., 2012, Pothole and channel system formation in the McMurdo Dry Valleys of Antarctica: New insights from cosmogenic nuclides: Earth and Planetary Science Letters, v. 355–356, p. 341–350, http://dx.doi.org/10.1016/j.epsl.2012.08.017

Niedermann, S., Graf, T., and Marti, K., 1993, Mass spectrometric identification of cosmic-ray-produced neon in terrestrial rocks with multiple neon components: Earth and Planetary Science Letters, v. 118, n. 1–4, p. 65–73, http://dx.doi.org/10.1016/0012-821X(93)90159-7

Nishiizumi, K., Imamura, M., Caffee, M. W., Southon, J. R., Finkel, R. C., and McAninch, J., 2007, Absolute calibration of 10Be AMS standards: Nuclear Instruments and Methods in Physics Research Section B: Beam Interactions with Materials and Atoms, v. 258, n. 2, p. 403–413, http://dx.doi.org/10.1016/j.nimb.2007.01.297

Putnam, A. E., Schaefer, J. M., Barrell, D. J. A., Vandergoes, M., Denton, G. H., Kaplan, M. R., Finkel, R. C., Schwartz, R., Goehring, B. M., and Kelley, S. E., 2010, *In situ* cosmogenic ^{10}Be production-rate calibration from the Southern Alps, New Zealand: Quaternary Geochronology, v. 5, n. 4, p. 392–409, http://dx.doi.org/10.1016/j.quageo.2009.12.001

Rignot, E., Mouginot, J., and Scheuchl, B., 2011a, Antarctic Grounding Line Mapping from Differential Satellite Radar Interferometry: Geophysical Research Letters, v. 38, n. 10, L10504, http://dx.doi.org/10.1029/2011GL047109

——— 2011b, MEaSUREs Antarctic Grounding Line from Differential Satellite Radar Interferometry: Boulder, Colorado, USA: NASA DAAC at the National Snow and Ice Data Center, http://dx.doi.org/10.5067/MEASURES/CRYOSPHERE/nsidc-0498.001

Schmidt, D. L., Williams, P. L., and Nelson, W. H., 1978, Geologic map of the Schmidt Hills quadrangle and part of the Gambacorta Peak quadrangle, Pensacola Mountains, Antarctica: United States Geological Survey, scale 1:250,000.

Shuster, D. L., and Farley, K. A., 2005, Diffusion kinetics of proton-induced ^{21}Ne, ^{3}He, and ^{4}He in quartz: Geochimica et Cosmochimica Acta, v. 69, n. 9, p. 2349–2359, http://dx.doi.org/10.1016/j.gca.2004.11.002

Stone, J. O., 2000, Air pressure and cosmogenic isotope production: Journal of Geophysical Research: Solid Earth, v. 105, n. B10, p. 23753–23759, http://dx.doi.org/10.1029/2000JB900181

——— 2004, Extraction of Al and Be from quartz for isotopic analysis: UW Cosmogenic Nuclide Lab Methods and Procedures, available online- http://depts.washington.edu/cosmolab/chem.shtml

Stone, J. O., Balco, G. A., Sugden, D. E., Caffee, M. W., Sass, L. C., III, Cowdery, S. G., and Siddoway, C., 2003, Holocene deglaciation of Marie Byrd Land, west Antarctica: Science, v. 299, n. 5603, p. 99–102, http://dx.doi.org/10.1126/science.1077998

Sugden, D. E., Balco, G., Cowdery, S. G., Stone, J. O., and Sass, L. C., III, 2005, Selective glacial erosion and weathering zones in the coastal mountains of Marie Byrd Land, Antarctica: Geomorphology, v. 67, n. 3–4, p. 317–334, http://dx.doi.org/10.1016/j.geomorph.2004.10.007

Todd, C., Stone, J., Conway, H., Hall, B., and Bromley, G., 2010, Late Quaternary evolution of Reedy Glacier, Antarctica: Quaternary Science Reviews, v. 29, n. 11–12, p. 1328–1341, http://dx.doi.org/10.1016/j.quascirev.2010.02.001

Tremblay, M. M., Shuster, D. L., and Balco, G., 2014a, Cosmogenic noble gas paleothermometry: Earth and Planetary Science Letters, v. 400, p. 195–205, http://dx.doi.org/10.1016/j.epsl.2014.05.040

——— 2014b, Diffusion kinetics of ^{3}He and ^{21}Ne in quartz and implications for cosmogenic noble gas paleothermometry: Geochimica et Cosmochimica Acta, v. 142, p. 186–204, http://dx.doi.org/10.1016/j.gca.2014.08.010

Vermeesch, P., Baur, H., Heber, V. S., Kober, F., Oberholzer, P., Schaefer, J. M., Schlücter, C., Strasky, S., and Wieler, R., 2009, Cosmogenic ^{3}He and ^{21}Ne measured in quartz targets after one year of exposure in the Swiss Alps: Earth and Planetary Science Letters, v. 284, n. 3–4, p. 417–425, http://dx.doi.org/10.1016/j.epsl.2009.05.007

Vermeesch, P., Balco, G., Blard, P. H., Dunai, T. J., Kober, F., Niedermann, S., Shuster, D. L., Strasky, S., Stuart, F. M., Wieler, R., and Zimmermann, L., 2015, Interlaboratory comparison of cosmogenic ^{21}Ne in quartz: Quaternary Geochronology, v. 26, p. 20–28, http://dx.doi.org/10.1016/j.quageo.2012.11.009

Wolf, R. A., Farley, K. A., and Kass, D. M., 1998, Modeling of the temperature sensitivity of the apatite (U–Th)/He thermochronometer: Chemical Geology, v. 148, n. 1–2, p. 105–114, http://dx.doi.org/10.1016/S0009-2541(98)00024-2

Young, N. E., Schaefer, J. M., Briner, J. P., and Goehring, B. M., 2013, A ^{10}Be production-rate calibration for the Arctic: Journal of Quaternary Science, v. 28, n. 5, p. 515–526, http://dx.doi.org/10.1002/jqs.2642